AD-778 487

AN ANALYTICAL AND EXPERIMENTAL INVESTIGATION OF HYPERSONIC VISCOUS INTERACTION PRESSURE EFFECTS

Neil J. Sliski

Air Force Flight Dynamics Laboratory
Wright-Patterson Air Force Base, Ohio

November 1973

AD 778487

DOCUMENT CONTROL DATA · R & D

(Security classification of title, body of abstract and indexing annotation must be entered when the overall report is classified)

1. ORIGINATING ACTIVITY (Corporate author)	2a. REPORT SECURITY CLASSIFICATION
Air Force Flight Dynamics Laboratory Wright-Patterson Air Force Base, Ohio 45433	UNCLASSIFIED
	2b. GROUP

3. REPORT TITLE

AN ANALYTICAL AND EXPERIMENTAL INVESTIGATION OF HYPERSONIC VISCOUS INTERACTION PRESSURE EFFECTS

4. DESCRIPTIVE NOTES (Type of report and inclusive dates)
Final Report, July 1970 - August 1971

5. AUTHOR(S) (First name, middle initial, last name)
Neil J. Sliski

6. REPORT DATE	7a. TOTAL NO. OF PAGES	7b. NO. OF REFS
November 1973	86	34

8a. CONTRACT OR GRANT NO.	9a. ORIGINATOR'S REPORT NUMBER(S)
b. PROJECT NO. 1366	AFFDL-TR-73-58
c. Task No. 136603	9b. OTHER REPORT NO(S) (Any other numbers that may be assigned this report)
d.	

10. DISTRIBUTION STATEMENT

Approved for public release; distribution unlimited.

11. SUPPLEMENTARY NOTES	12. SPONSORING MILITARY ACTIVITY
	Air Force Flight Dynamics Laboratory Wright-Patterson Air Force Base, Ohio 45433

13. ABSTRACT

A series of experimental surface pressure tests were conducted on a sharp leading edge, flat plate model. The tests were performed in the AFFDL High Temperature Facility (HTF). Nominal test conditions were Mach number 10 and a freestream Reynolds number per foot ranging from 1.65×10^5 to 4.6×10^5. Angle of attack ranged from 0° to 20°. The reduced data are compared with several viscous interaction theories and with test results obtained in other facilities.

Reproduced by
NATIONAL TECHNICAL
INFORMATION SERVICE
U S Department of Commerce
Springfield VA 22151

DD FORM 1 NOV 65 **1473**

14. KEY WORDS	LINK A		LINK B		LINK C	
	ROLE	WT	ROLE	WT	ROLE	WT
Viscous Interaction						
Hypersonic Aerodynamics						
Sharp Flat Plate						
Binary Collision Scaling						
Surface Pressure						

NOTICE

When Government drawings, specifications, or other data are used for any
purpose other than in connection with a definitely related Government
procurement operation, the United States Government thereby incurs no
responsibility nor any obligation whatsoever; and the fact that the
government may have formulated, furnished, or in any way supplied the said
drawings, specifications, or other data, is not to be regarded by implication
or otherwise as in any manner licensing the holder or any other person
or corporation, or conveying any rights or permission to manufacture, use,
or sell any patented invention that may in any way be related thereto.

Copies of this report should not be returned unless return is required by
security considerations, contractual obligations, or notice on a specific
document.

ib

AN ANALYTICAL AND EXPERIMENTAL INVESTIGATION OF HYPERSONIC VISCOUS INTERACTION PRESSURE EFFECTS
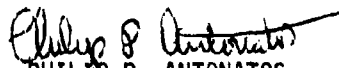
NEIL J. SLISKI

FOREWORD

This report was prepared by Neil J. Sliski of the High Speed Aero Performance Branch, Flight Mechanics Division, Air Force Flight Dynamics Laboratory, Wright-Patterson Air Force Base, Ohio. The work was performed under Project Number 1366, Task Number 136607.

This report was submitted by the author in October 1972.

The experimental pressure data were obtained in the AFFDL High Temperature Facility wind tunnel in July 1971.

The assistance of John E. Fehl for model design and fabrication, John F. Ford for instrumentation, Richard R. Smith, Everett M. Marshall, and James A. Funderburg for data reduction, and Richard D. Neumann for the initial suggestion are gratefully acknowledged.

This technical report has been reviewed and is approved.

PHILIP P. ANTONATOS
Chief, Flight Mechanics Division
Air Force Flight Dynamics Laboratory

ABSTRACT

A series of experimental surface pressure tests were conducted on a sharp leading edge, flat plate model. The tests were performed in the AFFDL High Temperature Facility (HTF). Nominal test conditions were Mach number 10 and a freestream Reynolds number per foot ranging from 1.65×10^5 to 4.6×10^5. Angle of attack ranged from 0° to 20°. The reduced data are compared with several viscous interaction theories and with test results obtained in other facilities.

TABLE OF CONTENTS

TABLE OF CONTENTS (CONT)

LIST OF ILLUSTRATIONS

LIST OF ILLUSTRATIONS (CONT)

AFFDL-TR-73-58

LIST OF ILLUSTRATIONS (CONT)

LIST OF ILLUSTRATIONS (CONT)

LIST OF TABLES

LIST OF SYMBOLS

b	Empirical constant. For wedge flow b = 3/4, see Eq.II-11
C	Chapman - Rubesin Parameter, $\quad C = \dfrac{\mu_w \, T_e}{\mu_e \, T_w}$
C_{f_e}	Local coefficient of friction, see Eq.II-15
C_p	Pressure coefficient, $C_p = \dfrac{p - p_\infty}{q_\infty}$
C'_p	Modified pressure coefficient, see Eq.II-10
$C^\star$	Chapman - Rubesin parameter based on a reference temperature, $$C^\star = \mu^\star \, T_e / \mu_e \, T^\star$$
d_{orig}	See Eq. 6
G	See Figure 2
G'	Wall temperature factor, see Eqs.II-28 and II-30
$\overline{H}$	Complete binary collision similarity parameter, see Eq. 26
I_1	See Eq. 12, and Figure 2
J_1	See Eq. 7
J_2	See Eq. 8
M	Mach Number
p	pressure
$p^{(o)}$	See Eq. 15, and Table II
$p^{(1)}$	See Eq. 15, and Table II
$p^{(2)}$	See Eq. 17
$p^{(3)}$	See Eq. 17

Pr	Prandtl number
q	dynamic pressure, $q = \frac{1}{2}\rho u^2$
r	recovery factor
R	Gas constant. For air $R = 1716.46(FT^2/Sec^2 - °R)$
Re	Reynolds number
T	Temperature
U	Velocity
$\bar{V}$	Hypersonic rarefaction parameter, $\bar{V} = \bar{X}/M^2$
X	Streamwise distance measured from the flat plate leading edge
X*	Transformed streamwise coordinate, See Eq. 20
$\bar{X}$	Hypersonic Viscous interaction parameter modified by the Chapman-Rubesin Reference Temperature Parameter, $\bar{X} = M_e^3 \sqrt{C^*/Re_{e_x}}$
α	Temperature correlation factor, $\alpha = \left[1 + 2.6 \left(T_w/T_0 \right) \right]$
β	Falkner-Skan pressure gradient parameter, $\beta = (\gamma - 1)/\gamma$
γ	Specific heat ratio
δ	Angle of attack, See Eq. II-2
δ_1	Boundary layer thickness
δ^*	Boundary layer displacement thickness
θ	Boundary layer momentum thickness
μ	Viscosity
ρ	Density
τ	Shearing Stress, See Eq. II-15
ω	Exponent in viscosity-temperature relation, $\mu/\mu_\infty = (T/T_\infty)^\omega$

Subscripts

aw	Adiabatic wall
e	Inviscid conditions at body surface
inc	incompressible value
inv	inviscid value
o	stagnation value
w	wall conditions
x	based on streamwise distance from the leading edge
X*	Based on transformed streamwise distance from the leading edge
∞	Freestream conditions in the undisturbed flow field upstream of the model

Superscripts

*	Reference Temperature Value

SECTION I

INTRODUCTION

At hypersonic speeds, the deceleration of the fluid by the viscous processes in a boundary layer generally produces very high temperatures. One result of these high temperatures is an increase in the thickness of the boundary layer over the thickness encountered at the same freestream Reynolds number at lower speeds. This increased boundary layer thickness results in a significant change in the effective body shape which in turn generates large induced pressures. These pressures are transmitted to the inviscid shocklayer thereby altering the shockwave strength and shape. This interaction between boundary layer and shockwave is commonly referred to as a viscous interaction.

Viscous interaction is one of a number of important high speed phenomena that require proper evaluation prior to making any realistic aerodynamic performance estimate for a high speed vehicle. It is the purpose of this report to experimentally determine the accuracy of interaction theories based on: (1) the classical hypersonic viscous interaction parameter, $\bar{X}$, originally formulated by Lees and Probstein (Reference 12), and (2) the binary collision scaling parameter, $(\rho_\infty X^*)^{-1/2}$, due to the work of Harney (Reference 20).

Data was obtained by conducting a series of wind tunnel tests on a sharp leading edge flat plate model in the AFFDL High Temperature Facility (HTF). Nominal test conditions were Mach number 10 and a freestream Reynolds number ranging from 1.65×10^5 to 4.6×10^5 per foot. Angle of attack ranged from 0° to 20°. The reduced data are compared with several viscous interaction theories and with test results obtained in other facilities.

The present study is limited to the classical regime of viscous interaction where continuum theory and no-slip boundary conditions apply. Neither the leading edge problem nor molecular effects are considered. A preliminary report on the test is presented in Reference 1.

SECTION II

TEST EQUIPMENT DESCRIPTION

1. AFFDL HIGH TEMPERATURE FACILITY (HTF)

The HTF is a blowdown wind tunnel which operates at a nominal Mach number of 10. Stagnation temperatures from 2200°R to 3500°R are generated by an alumina dioxide pebble bed storage heater. Stagnation pressures may be varied from 100 to 600 psia. The tunnel operates intermittently with nominal run times of 2 to 3 minutes, depending upon the mass flow into the vacuum system. It has an open jet test section with a nominal 15 inch diameter test core.

The basic design of the wind tunnel and its physical characteristics are presented in References 2 and 3. The nozzle system described in these reports has been modified and a new diffuser has been designed to match the enlarged nozzle exit diameter.

The test was conducted using a contoured nozzle having a 0.861-inch throat diameter and a 24-inch exit diameter. Nominal test section Mach number was 10. Reservoir pressures were varied from 200 to 500 psia.

2. EXPERIMENTAL FLAT PLATE MODEL

A sketch of the pressure model showing the location of the 10 pressure taps and one thermocouple is presented in Figure 1.

The model is made of 15-4PH stainless steel. The leading edge was held to a maximum radius of .002 inches. The top, bottom, and sloping front surfaces are 1/8-inch thick and are supported by a 1/2-inch thick C-frame. Both surfaces are silver soldered to a copper water jacket. The model was cooled during the test to minimize transpiration effects due to a temperature differential between the model surface and the transducer.

2

TAP	X (IN)
1	0.6
2	0.8
3	1.0
4	1.2
5	1.4
6	1.6
7	1.8
8	2.2
9	2.6
10	3.0

10 TAPS
.069 ± .001 I.D.

X

IRON CONSTANTAN
THERMOCOUPLE

3

6

.5

.8

Scale: 1/2

2.2

2.9

6.5
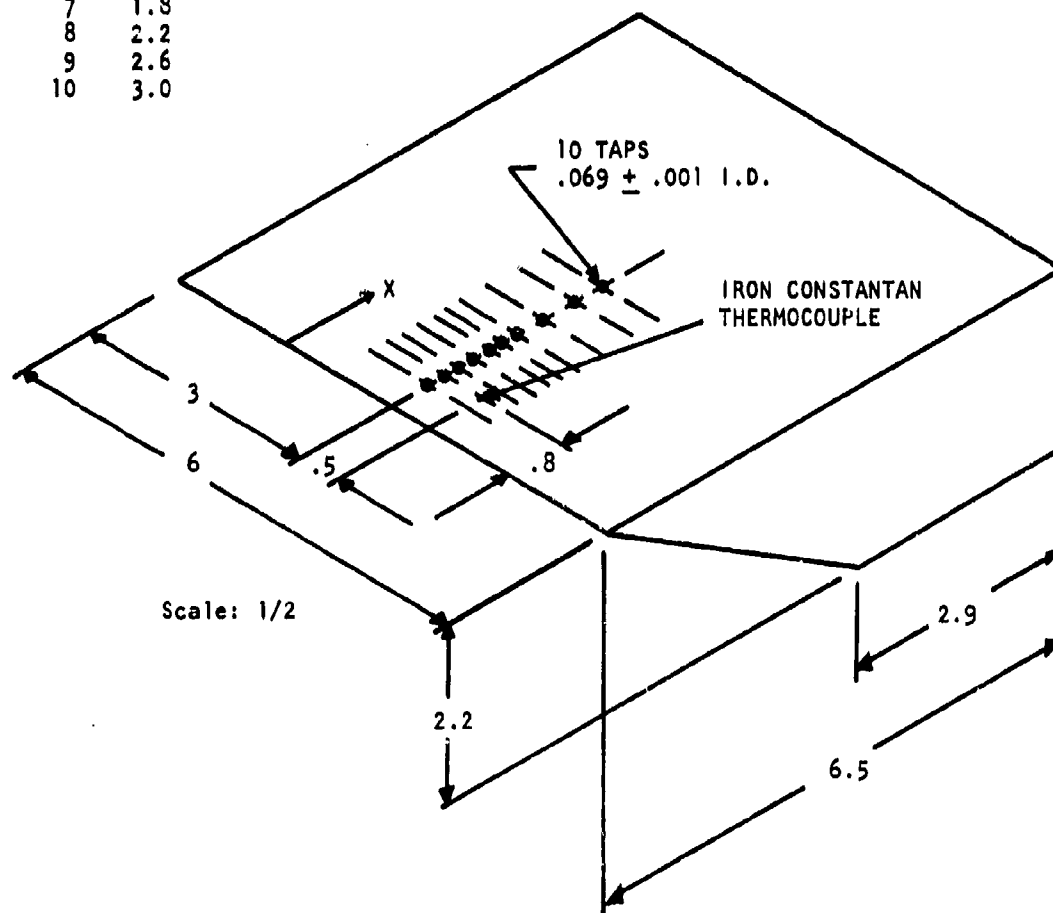
Figure 1. Flat Plate Pressure Model Three
Dimensional View

3

3. INSTRUMENTATION

Surface pressures were measured directly by ten Consolidated Control Corporation Ultradyne Pressure Transducers. In the pressure range tested, quoted laboratory accuracy is $\pm$ 0.1% RMS of the full range. In the present case this amounts to $\pm$ 0.0156 mm Hg over the range 0.4 to 16 mm Hg. Each transducer was connected to a model orifice by 30 inches of 0.140" O. D. x 0.120" I. D. stainless steel tubing and 125 inches of 0.0938 ID copper tubing. Transducer output was amplified by 3 KHZ carrier amplifiers manufactured by Natel Engineering Company. The amplified signals were then digitized by a Control Data Corporation 8032C analog/digital converter and stored on magnetic tape.

One iron/constantan thermocouple was used to measure the surface temperature. Originally, two thermocouples were available; however, one was damaged after the model was assembled and before it was tested.

SECTION III

METHOD OF DATA REDUCTION

1. TEST SECTION CONDITIONS

For the test conditions run, it is permissable to use the thermally perfect air approximation as described in Reference 4. This method has been incorporated in a CDC 160A computer program. Temperature and pressure fluctuation corrections to Mach number have been estimated from AEDC wind tunnel correction data (see References 2 and 3). A summary of the test conditions for which data were obtained is presented in Table I.

2. FLAT PLATE PRESSURE MEASUREMENTS

The output signals of the pressure transducer and thermocouple amplifiers were digitized and stored on magnetic tape. A CDC 160A computer was used to put the fundamental data onto computer cards. The data were subsequently used as input data to a CDC 6600 computer program that performed the final data reduction and compared the experimental results with theoretical predictions.

3. TEST PROCEDURE

After the wind tunnel reached the nominal test condition, the model was injected into the flow field and rotated to the proper angle of attack. Then data was taken at 15 sec intervals until the tunnel flow broke down. The raw data were examined for constancy of P_∞, P_w, and T_w. The test point judged to be most representative of the data taken was reduced and compared with the various viscous interaction theories.

All of the data shown in this report were taken only after the surface temperature of the water-cooled model had equilibrated and the pressures had stabalized. This point was usually reached after the model had been exposed to the flow 60 to 90 seconds. Therefore, any tubulation lag time effects on the measured pressures should be minimal.

However, a certain amount of surge in the wind tunnel, on the order of $\pm$ 1% in P_∞, did occur. The effect of this nonsteady flow is discussed in more detail in Section V.

The repeatability, consistency, and lack of scatter in the data tend to substantiate the quoted accuracy of the pressure transducers and their associated amplifiers.

TABLE I

SUMMARY OF AFFDL TEST CONDITIONS

Figure No.	δ_{inv} (DEG)	P_o (PSIA)	T_o (°R)	M_∞	Re_∞/FT x 10^{-5}	T_w (°R)
3,7	0	197.2	2374	9.82	1.68	709
	0	199.7	2277	9.90	1.81	669
	0	298.7	2422	9.89	2.41	710
	0	503.5	2460	9.92	3.92	711
	0	504.1	2494	9.93	3.81	707
10,11	5.11	496.8	2388	9.71	4.34	753
	5.11	301.5	2340	9.72	2.72	734
	5.12	200.9	2334	9.59	1.89	723
12,13	10.12	504.4	2331	9.73	4.60	773
	10.12	300.8	2388	9.73	2.61	793
	10.13	201.0	2409	9.85	1.65	751
14,15	15.21	297.9	2226	9.95	2.78	816
16,17	15.28	502.7	2418	9.83	4.15	876*
18,19	11.19	500.0	2373	9.88	4.21	770
20,21	12.23	504.0	2368	10.04	4.08	828
22,23	13.21	504.1	2406	9.81	4.22	797
24,25	14.20	504.0	2407	10.00	4.00	870
26,27	17.25	503.9	2361	9.86	4.32	852
28,29	19.24	502.6	2352	10.01	4.16	851
30,31	20.20	503.8	2411	10.02	3.96	862

* This value represents the best estimate for T_w. A more exact value is not available because the thermocouple output saturated the capabilities of the CDC 8032C analog to digital converter.

SECTION IV

REVIEW OF THEORY

1. DERIVATION OF BASIC PARAMETERS

In the development of the classical weak and strong interaction theories, the need arises for a representative value of $\rho\mu$ within the boundary layer. This can be done once a suitable reference temperature, $T*$, is established. The choice of a suitable reference temperature is most important, and in the past many different methods have been used to determine $T*$. Chapman and Rubesin (Reference 5) proposed using the wall temperature. Monaghan (Reference 6) used a function based on a relation developed by Crocco (Reference 7),

$$T* = \frac{T_0}{6}\left[1 + 3\left(\frac{T_w}{T_0}\right) + 2\left(\frac{T_e}{T_0}\right)\right] \tag{1}$$

Cheng (Reference 8) simplified the Monaghan function by assuming the ratio of the temperature at the boundary layer edge to total temperature to be neglibible,

$$T* = \frac{T_0}{6}\left[1 + 3\left(\frac{T_w}{T_0}\right)\right] \tag{2}$$

Eckert (Reference 9) chose a function based on a semiempirical derivation,

$$T* = \frac{T_0}{6}\left[1.32r + 3\left(\frac{T_w}{T_0}\right) + (3 - 1.32r)\left(\frac{T_e}{T_0}\right)\right] \tag{3}$$

This equation reduces exactly to Monaghan's if the recovery factor, r, is set equal to $1/1.32$.

In this report the Eckert reference temperature is chosen as being more meaningful when local flat plate similarity exists. By employing a linear viscosity-temperature relation, the appropriate $\rho\mu$ ratio is determined.

The largest drawback in applying the Eckert formula is the need to calculate the recovery factor. For laminar flow the recovery factor is taken to be

$$r^* = \sqrt{P_r^*} \tag{4}$$

where the Prandtl number, P_r^*, is calculated at the reference temperature. Details are contained in Appendix I for the calculation of P_r^*.

2. VISCOUS INTERACTION PRESSURE THEORIES

A number of theories are available in the literature which are pertinent to the viscous interaction problem. The earliest work is contained in several closely related studies by Lees (References 10 and 11), Lees and Probstein (References 12 and 13), Bertram (Reference 14), and Li and Nagamatsu (Reference 15). The results were summarized by Hays and Probstein (Reference 16).

The classical weak and strong viscous interaction formulations, based on similarity concepts and presented herein, are from Reference 16. Additional theories, put forth by Moore (Reference 17) and Dewey (Reference 18), based on the concept of locally similar flows are also noted.

In addition the binary collision scaling concept, originally proposed by Birkhoff (Reference 19) and applied to the viscous interaction problem by Harney (Reference 20) and by Harney and Petrie (References 21 and 22), is given. Although Harney developed the binary collision scaling approach to show that a meaningful similitude exists in very high energy, dissociated, nonequilibrium, frozen air flows, the theory is applicable to lower energy air flows and is presented for comparison.

a. Classical, Second Order, Weak Interaction

The phenomenon of weak viscous interaction has been reported in References 10 through 18. Reference 16, which is widely available, gives

9

the formulation:

$$\frac{p}{p_e} = 1 + \gamma\left(\frac{M_\infty}{M_e}\right) J_1 d_{orig} \bar{X} + \frac{\gamma(\gamma + 1)}{4}\left(\frac{M_\infty}{M_e}\right)^2 J_2 d_{orig}^2 \bar{X}^2 \quad (5)$$

For $P_r = 0.725$

$$d_{orig} = \frac{.968}{M_e^2}\left(\frac{T_w}{T_e}\right) + .145\ (\gamma - 1) \quad (6)$$

This d_{orig} is based on the Crocco reference temperature. For an alternate version of d_{orig} based on the Eckert reference temperature see Appendix I, Section 4.

$$J_1 = \left(\frac{p_\infty}{p_e}\right)\left[\left(\frac{\gamma + 1}{2}\right)(M_\infty \delta_{inv}) + \frac{1 + 2\left(\frac{\gamma + 1}{4}\right)^2 (M_\infty \delta_{inv})^2}{\sqrt{1 + \left(\frac{\gamma + 1}{4}\right)^2 (M_\infty \delta_{inv})^2}}\right] \quad (7)$$

$$J_2 = \left(\frac{p_\infty}{p_e}\right)\left\{1 + \frac{\left(\frac{\gamma + 1}{4}\right)(M_\infty \delta_{inv})\left[\left(\frac{\gamma + 1}{4}\right)^2 (M_\infty \delta_{inv})^2 - \frac{3}{2}\right]}{\left[1 + \left(\frac{\gamma + 1}{4}\right)^2 (M_\infty \delta_{inv})^2\right]^{3/2}}\right\} \quad (8)$$

$$\bar{X} = \frac{M_e^3 \sqrt{C^*}}{\sqrt{Re_{e_x}}} \quad (9)$$

The (p_∞/p_e) ratio encountered in Equations 7 and 8 is to be determined from tangent-wedge theory (see Appendix II, Equation II-1).

b. Classical, Zeroth Order, Strong Interaction $(\delta_{inv} = C°)$

As in the weak interaction case, strong viscous interaction has been investigated theoretically in References 10 through 18. The result, as given in Reference 16, is

$$\frac{p}{p_\infty} = \frac{3}{8}\ (\gamma - 1)\sqrt{\gamma(\gamma + 1)}\ G\ \bar{X}\ . \quad (10)$$

10

The parameter G, which is a function of the Prandtl number, the specific heat ratio, and the temperature ratio, T_w/T_0, was determined from the values given in Table 9-2 of Reference 16, and is plotted in Figure 2. These values are essentially the same as those calculated by Li and Nagamatsu (Reference 23). They are based on the assumptions of unit Prandtl number, $\gamma = 1.4$, a Falkner-Skan pressure gradient function, β, equal to 0.286, and a linear viscosity - temperature relation, $\omega = 1$. Cheng (Reference 8) obtained much the same result for a Prandtl number of 3/4,

$$\frac{p}{p_\infty} = 0.332\sqrt{3} \ \frac{\gamma(\gamma-1)}{(\gamma+1)} \ \left[1 + 2.6\left(\frac{T_w}{T_0}\right)\right]\overline{X} . \tag{11}$$

Dewey (Reference 18) used the concept of local similarity to extend the range of viscous interaction theory to include the case where the Falkner-Skan parameter, β, is allowed to vary in the streamline direction, and the Prandtl number is not necessarily equal to unity. Other exact similarity restrictions were relaxed but they will not be considered here since they are not germane to the present problem. In the strong interaction limit to Dewey's solutions, the pertinent equation is

$$\frac{p}{p_\infty} = \frac{3}{8} \ (\gamma-1)\sqrt{\gamma(\gamma+1)} \ (\sqrt{2}\ I_1) \ \overline{X} \tag{12}$$

where I_1 was obtained from tables contained in Reference 18, and is presented in Figure 2.

Moore (Reference 17) used a modified local flat plate similarity concept to formulate solutions in both the weak and the strong interaction regions. His results using the simplified wall temperature factor, α, where

$$\alpha = \left[1 + 2.6\left(\frac{T_w}{T_0}\right)\right] , \tag{13}$$

correlate fairly well with more exact forms given in References 16, 18, and 23, and shown in Figure 2. Using this relation in place of G or $\sqrt{2}\ I_1$ the strong interaction limit to the similar solutions may be

11
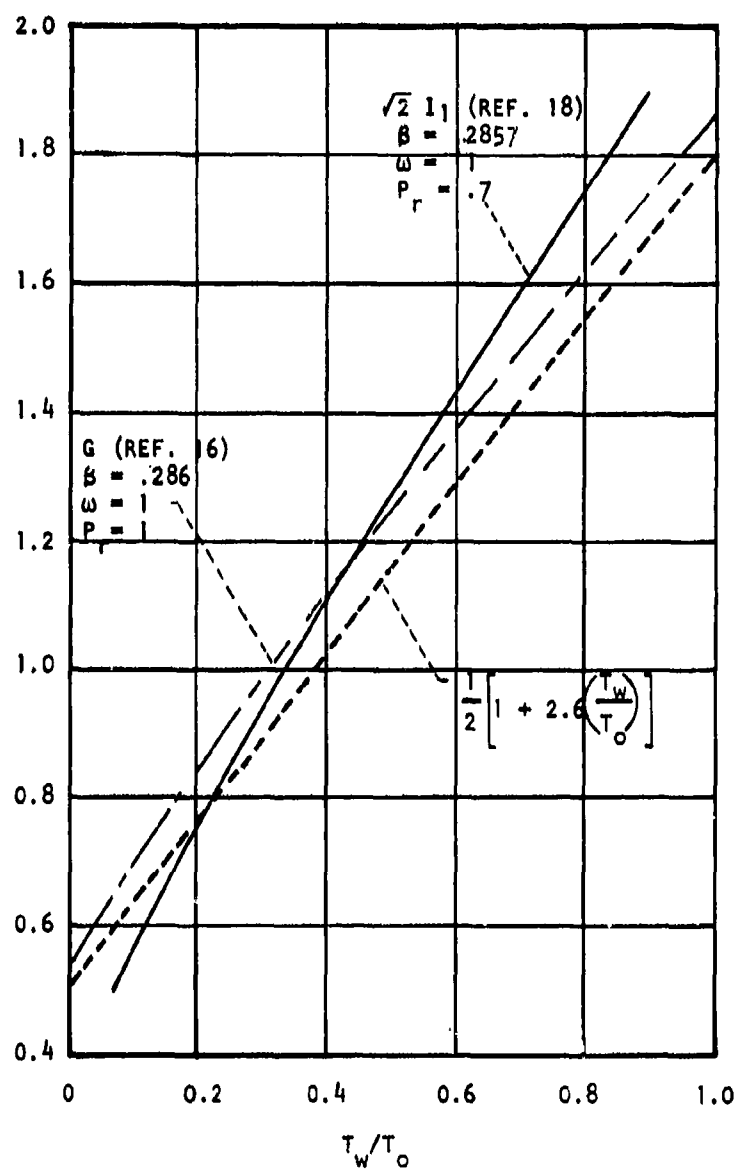
Figure 2. Comparison of Temperature Effect Relations
in the Strong Interaction Regime

written as

$$\frac{p}{p_\infty} = \frac{3}{8} \; (\gamma - 1) \; \sqrt{\gamma \, (\gamma + 1)} \left\{ \frac{1}{2} \left[1 + 2.6 \; \left(\frac{T_w}{T_0} \right) \right] \right\} \overline{X} \, . \qquad (14)$$

This corresponds to Dewey's result and compares favorably with Cheng's result (Eq. 11).

c. Classical, First Order, Strong Interaction ($\delta_{inv} = 0°$)

The only first order calculations that have been carried out are for the case of an insulated flat plate at zero degrees angle of attack with $P_r = 1$ and $\gamma = 1.4$. To the first order, the induced pressure on a flat plate is

$$\frac{p}{p_\infty} = p^{(1)} + p^{(0)} \overline{X} \qquad (15)$$

where $p^{(0)}$ and $p^{(1)}$ correspond to the zeroth and first order terms in an asymptotic series expansion representing the static pressure distribution along the outer edge of the boundary layer. Calculations for $p^{(0)}$ and $p^{(1)}$ have been carried out by many authors. The various results (Reference 24, Table I) are summarized in Table II. Rather than determine $p^{(1)}$ by solving the von Karman momentum integral relation (Reference 10), it is recognized tnat eventually the strong interaction region will transition to a weak interaction region where $p^{(1)}$ can be determined by equating the strong and weak solutions for various $\overline{X}$ and T_w/T_0 ratios. For $\gamma = 1.4$ and $P_r = 0.725$, $p^{(1)}$ varies from about 0.90 for $\overline{X} = 2$ and $T_w/T_0 = 0.2$ to about 0.98 for $\overline{X} = 0.5$ and $T_w/T_0 = 0.8$. These resu1ts are comparable to Lees (Reference 10) value of 0.92. Rather than select any derived value, $p^{(1)}$ is arbitrarily set equal to 1.0 since $p/p_\infty \longrightarrow 1$ as $\overline{X} \longrightarrow 0$. Little error is involved in making this rather arbitrary selection. As a result it may be postulated that in the strong interaction regime

$$\frac{p}{p_\infty} = 1 + \frac{3}{16} \; (\gamma - 1) \; \sqrt{\gamma(\gamma + 1)} \left[1 + 2.6 \left(\frac{T_w}{T_0} \right) \right] \overline{X} \qquad (16)$$

where the simplified temperature function is adopted in favor of the more complex functions G and I_1.

d. Classical, First Order, Strong Interaction ($\delta_{inv} > 0°$)

In the case of a sharp flat plate inclined at an angle of attack with respect to the freestream, the strong interaction result is (Reference 16)

$$\frac{p}{p_\infty} = p^{(0)} \overline{\chi} \left[1 + \frac{p^{(1)}(M_\infty \, \delta_{inv})}{\overline{\chi}^{1/2}} + \frac{p^{(2)} + p^{(3)}(M_\infty \, \delta_{inv})^2}{\overline{\chi}} \right] \qquad (17)$$

where $p^{(0)}$ and $p^{(1)}$ are the same as for the zero degree angle of attack equations. However, calculations beyond the zeroth order for the functions $p^{(2)}$ and $p^{(3)}$ have so far not been carried out. Therefore, no comparison between the first order, strong interaction solution and experimental data at angles of attack can be made.

e. Binary Collision Scaling Interaction

The classical viscous interaction formulation leads to the Probstein-Lees hypersonic, viscous interaction parameter, $\overline{\chi}$. The formulations by Birkhoff (Reference 19), Harney (Reference 20), and Harney and Petrie (References 21 and 22) lead to a description of hypersonic viscous interaction in terms of a binary collision scaling parameter, $(\rho_\infty \chi^*)^{-1/2}$. With this approach the hypersonic, small disturbance solution becomes (Appendix II, Equation II-36)

$$(18)$$

$$\left(c_p + \frac{p_\infty}{q_\infty} \right)^{\frac{1}{2}} \left(c_p - \frac{3}{4} \frac{p_\infty}{q_\infty} \right)^{\frac{1}{2}} = \left[1.015(1+\gamma) \right]^{\frac{1}{2}} \left[\left(c_p + \frac{p_\infty}{q_\infty} \right)^{\frac{1}{2}} \delta_{inv} + G'(\rho_\infty x^*)^{-\frac{1}{2}} \right]$$

TABLE II

COMPARISON OF STRONG INTERACTION THEORY ANALYSIS

FOR $\gamma = 1.4$ AND $T_w/T_o = 1$

$\dfrac{p}{p_\infty} = p^{(1)} + p^{(o)} \, \overline{\chi}_\infty$		
Theory	$p^{(o)}$	$p^{(1)}$
Stewartson	0.555	0.489
Oguchi	0.555	$0.194 \, \dfrac{\overline{\chi}_\infty^{1.525}}{M_\infty^{1.050}}$
Lees	0.52	0.92
Li & Nagamatsu	0.514	
Nagakura & Naruse	0.510	0.759
Cheng	$0.592 \left(\dfrac{\mu^*}{\mu_o}\right)^{1/2}$	
Mann & Bradley		0.8
Aroesty		$-0.26 \, (\overline{\chi}_\infty^{3/2}/M_\infty)$
Galkin	0.505	$-0.101 \, (\overline{\chi}_\infty^{3/2}/M_\infty)$
Tien	0.528	0.743
Pan & Probstein	0.651	

Appendix II shows that the approximate result (Equation II-30) for the secondary correlation factor, G', corresponds very closely with the more complex exact solution, Equation II-28. The approximate result is

$$G' = 3.84 \times 10^{-6} \left[1 + 2.6 \left(\frac{T_w}{T_0} \right) \right]^{3/4} \tag{19}$$

The stretched axial coordinate transformation, X^*, that produces local flat plate similarity in the presence of small disturbance pressure gradients is

$$X^* = p \int_0^X \frac{1}{p} \, dx \tag{20}$$

In the strong interaction limit $X^*/X = 2/3$, whereas in the weak interaction limit $X^* = X$. A useful linearized approximation for departures from the strong interaction limit is (Reference 20)

$$\frac{X^*}{X} = \frac{2}{3} \left[1 + \frac{1}{4} \left(\frac{p_\infty}{p - p_\infty} \right) \right] \tag{21}$$

(1) $\delta_{inv} = 0°$

For the case of a flat plate, Equation 18 reduces to a quadratic expression for the weak and strong interaction limits, and to a cubic expression for the linearized approximation for departures from the strong interaction limit. However, as is pointed out in Appendix III, the exact solutions are not as satisfactory as the approximate solutions. Therefore, the approximate solution is adopted on the grounds that it was derived from a consistent set of assumptions.

$$c_p = \left[1.015 (1 + \gamma) \right]^{1/2} G' (p_\infty X^*)^{-1/2} \tag{22}$$

The appropriate $X^* - X$ relation is applied to obtain solutions for the weak, linearized, and strong interaction limits in Appendix III.

(a) Weak Interaction Limit Solution, $X^* = X$

$$C_p = \left[1.015 \, (1 + \gamma) \right]^{\frac{1}{2}} \, \bar{\chi}' \, (\rho_\infty X)^{-\frac{1}{2}} \tag{23}$$

(b) Linearized Departure Solution, $X^* = \frac{2}{3} X \left[1 + \frac{1}{4} \left(\frac{p_\infty}{p - p_\infty} \right) \right]$

$$C_p = \sqrt{ \left(\frac{1}{8} \frac{p_\infty}{q_\infty} \right)^2 + \frac{3}{2} \left[1.015 \, (1 + \gamma) \right] \, \bar{\chi}'^{2} / (\rho_\infty X) } - \left(\frac{1}{8} \frac{p_\infty}{q_\infty} \right) \tag{24}$$

(c) Strong Interaction Limit Solution, $X^* = 2 X/3$

$$C_p = \sqrt{\frac{3}{2}} \left[1.015 \, (1 + \gamma) \right]^{\frac{1}{2}} \, \bar{\chi}' \, (\rho_\infty X)^{-\frac{1}{2}} \tag{25}$$

(2) $\delta_{inv} > 0°$

In the case of a wedge inclined to the freestream, it is not possible to discount the $\frac{p_\infty}{q_\infty}$ term as in the $\delta_{inv} = 0°$ case because of the importance of the $(C_p + p_\infty/q_\infty)^{1/2} \delta_{inv}$ term on the right hand side of Equation 18. Therefore, due to the complex nature of this equation, an iterative technique must be used. This was accomplished on a CDC - 6600 digital computer.

It is apparent from Equations 19, 23, 24, and 25, that combining the wall temperature effect and binary collision interaction effect into one unified correlation parameter is possible. This parameter is designated $\overline{H}$ and is used as the independent variable in the plots of C_p in the figures.

$$\overline{H} = \left[1 + 2.6 \left(\frac{T_w}{T_o} \right) \right]^{3/4} (\rho_\infty X)^{-1/2} \tag{26}$$

17

SECTION V

DISCUSSION

In the literature, numerous theories for predicting the effects of viscous interaction can be found. Rather than attempt to compare each theory, many of which differ only slightly, this report limits itself to considering only the classical, second order, weak (Equation 5) and first order, strong (Equation 16) interaction solutions in addition to the binary collision scaling analysis. In both the classical and binary collision theories, a secondary, temperature-dependent correlation parameter is encountered in addition to the primary correlation parameters $\overline{X}$ and $(\rho_\infty X^*)^{-1/2}$, respectively. When comparing the classical analysis to experiment, the simplified temperature function $1/2\,\alpha$ (Equation 13) is used in this report instead of the more complex relations G and $\sqrt{2}\,I_1$, presented in References 16 and 18.

In the binary collision scaling analysis, a similar function, designated G' is encountered. Harney (Reference 20), with the aid of a number of simplifying assumptions, was able to arrive at a function dependent only on the wall-to-total-temperature ratio (Equation 19). In Appendix II, the approximate values for G' are shown to agree remarkably well with the more exact values afforded by Equation II-28. Therefore, the approximate equation, being both accurate and simple, is used in this report for data correlation.

A summary of the wind tunnel conditions that were run in the AFFDL tests is presented in Table I.

Table III contains an identification code to be used in relating the theoretical results of Section IV to the experimental data presented in Figures 3 through 31.

The analysis is divided into two parts, one for the flat plate oriented parallel to the freestream, and one for the flat plate inclined at an angle of attack to the freestream.

18

TABLE III

THEORY IDENTIFICATION CODE*
FOR USE WITH FIGURES 3 THROUGH 31

Code	Type of Interaction Theory	Equation $(\delta_{1inv} \equiv 0°)$	Equation $(\delta_{1inv} \gtrless 0°)$
WI	Classical, Second Order, Weak (d_{orig} from Equation 6)	5	5
WIE	Classical, Second Order, Weak (d_{orig} from Equation I-14)	5	5
SI	Classical, First Order, Strong	16	-
BCW	Binary Collision, Weak	23	18
BCL	Binary Collision, Linearized	24	18
BCS	Binary Collision, Strong	25	18

*The term "INV" encountered in these figures refers to the inviscid, perfect gas results for wedges at various angles of attack (Reference 4).

1. FLAT PLATE PARALLEL TO THE FREESTREAM ($\delta_{inv} = 0°$)

In Figure 3 results of the AFFDL zero degree angle of attack tests are compared with the classical, second order, weak interaction, and first order, strong interaction theories. Kendall's experimental results (Reference 25) are compared with the classical theories in Figure 4, while results from Bertram's experiments are shown in Figures 5 and 6. In Figures 7, 8, and 9 the data of Figures 3,4, and 5 are compared with the predictions of binary collision theory.

In the derivation of the classical and binary collision theories, fairly restrictive restraints are imposed on the magnitude of $M_\infty \delta$. The effective angle of attack, δ, is the sum of the geometric angle of attack, δ_{inv}, plus the induced angle of attack attributable to the boundary layer displacement effect.

$$\delta = \delta_{inv} + \frac{d\delta^*}{dx} \tag{27}$$

The classical, strong pressure interaction region is characterized by the hypersonic, strong shock limitation,

$$(M_\infty \delta)^2 \gg 1 \tag{28}$$

whereas the classical, weak interaction regime is characterized by

$$(M_\infty \delta)^2 \ll 1 \tag{29}$$

The only limitation on the binary collision analysis is that

$$(M_\infty \delta) \geq 1 \tag{30}$$

which is less restrictive than the classical limitations.
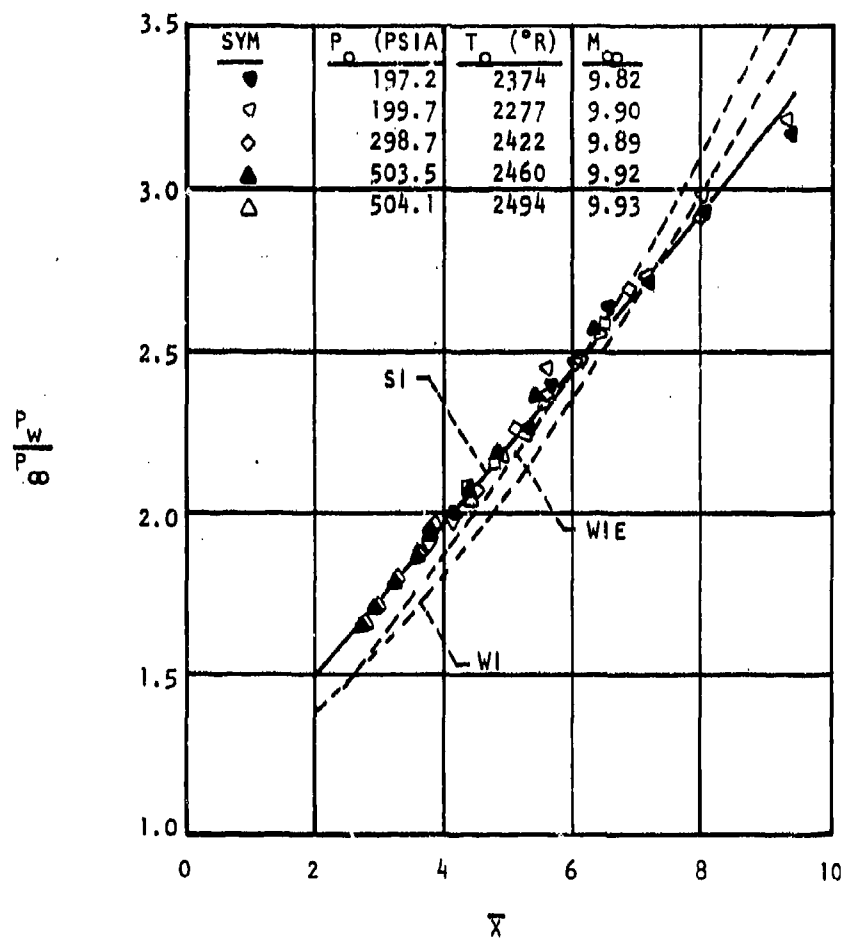
Figure 3. Comparison of Classical Interaction Theory
with Experimental Pressure Distribution on
the AFFDL Flat Plate at $\delta_{inv} = 0°$
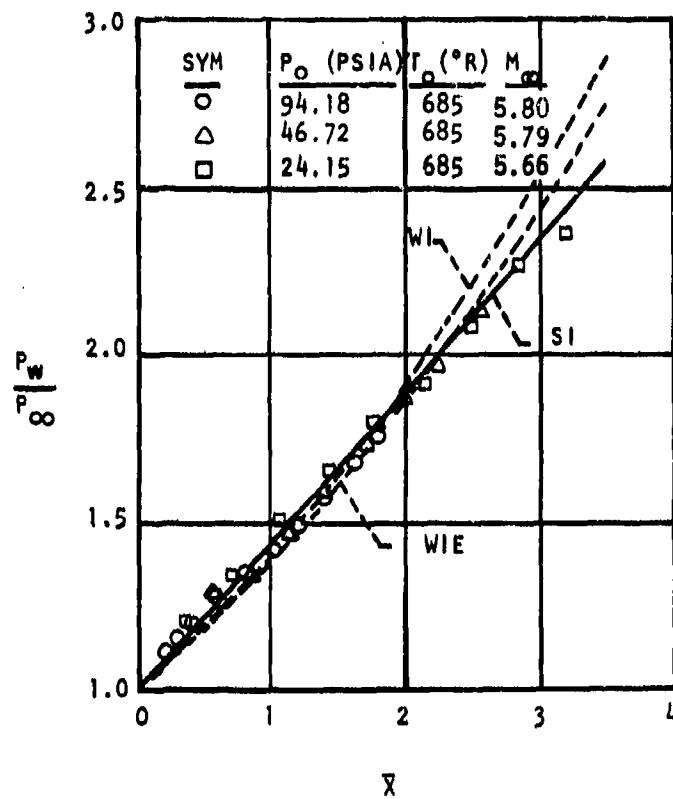
Figure 4. Comparison of Classical Interaction Theory with Experimental Pressure Distribution on Kendall's Flat Plate at $\delta_{inv} = 0°$
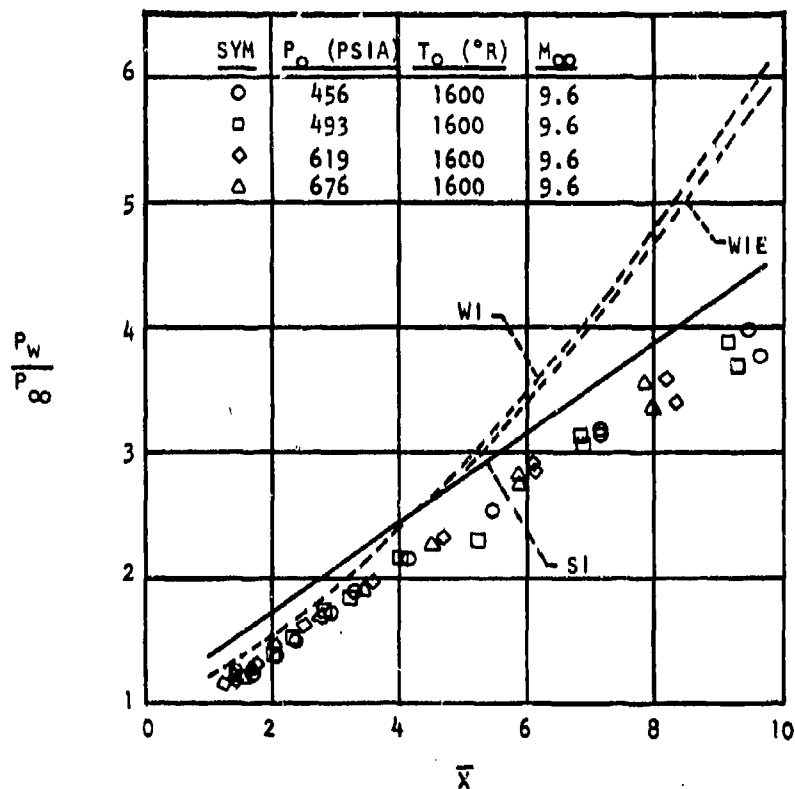
Figure 5. Comparison of Classical Interaction Theory with Experimental Pressure Distribution on Bertram's Flat Plate at $\delta_{inv} = 0°$
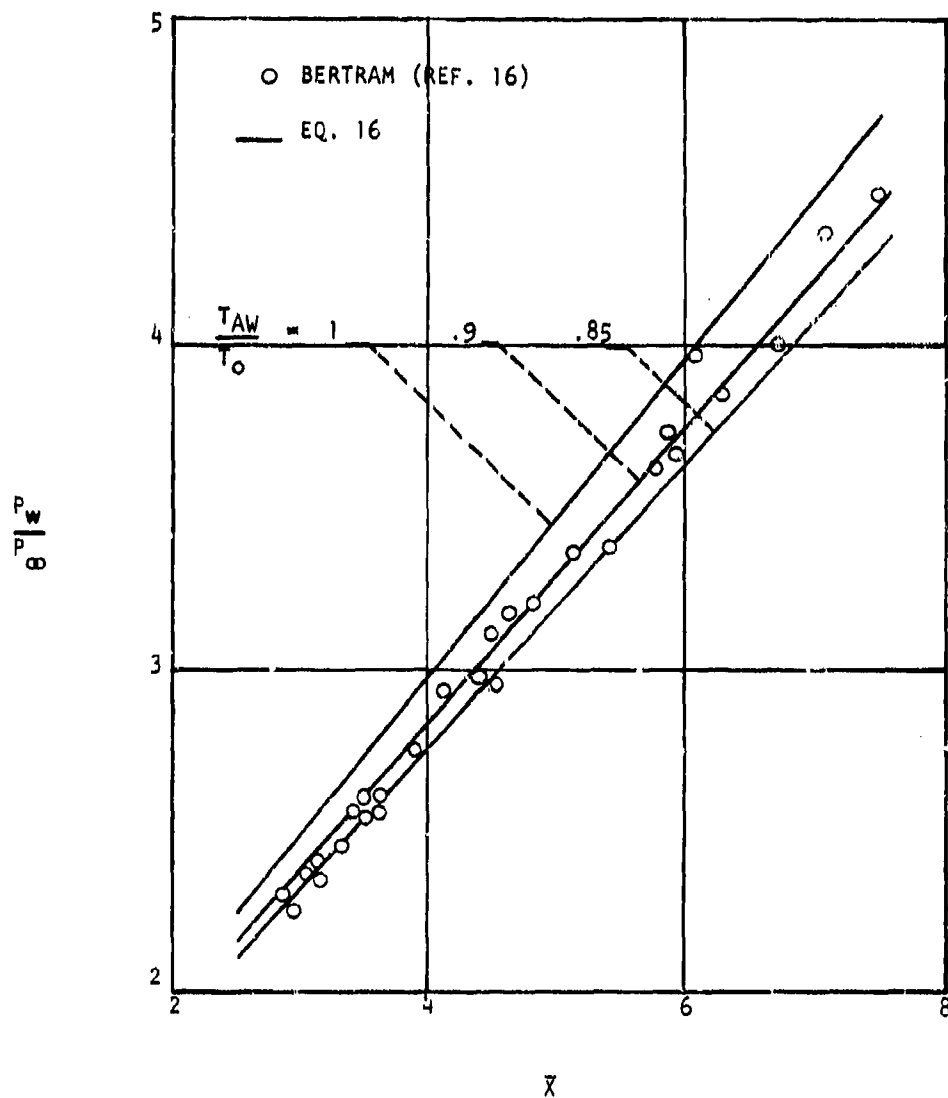
Figure 6. Comparison of Classical Interaction Theory
with Experimental Pressure Distribution on
Bertram's Insulated Flat Plate at δ_{inv} = 0°
(from Ref. 16)
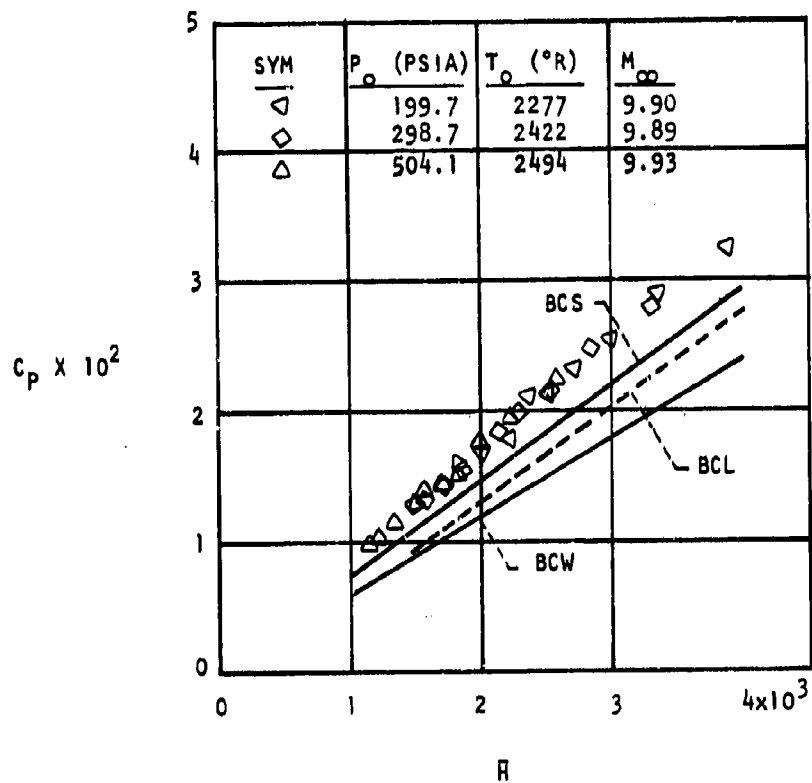
Figure 7. Comparison of Binary Collision Interaction
Theory with Experimental Pressure Coefficient
on the AFFDL Flat Plate at $\delta_{inv} = 0°$

$C_p \times 10^2$
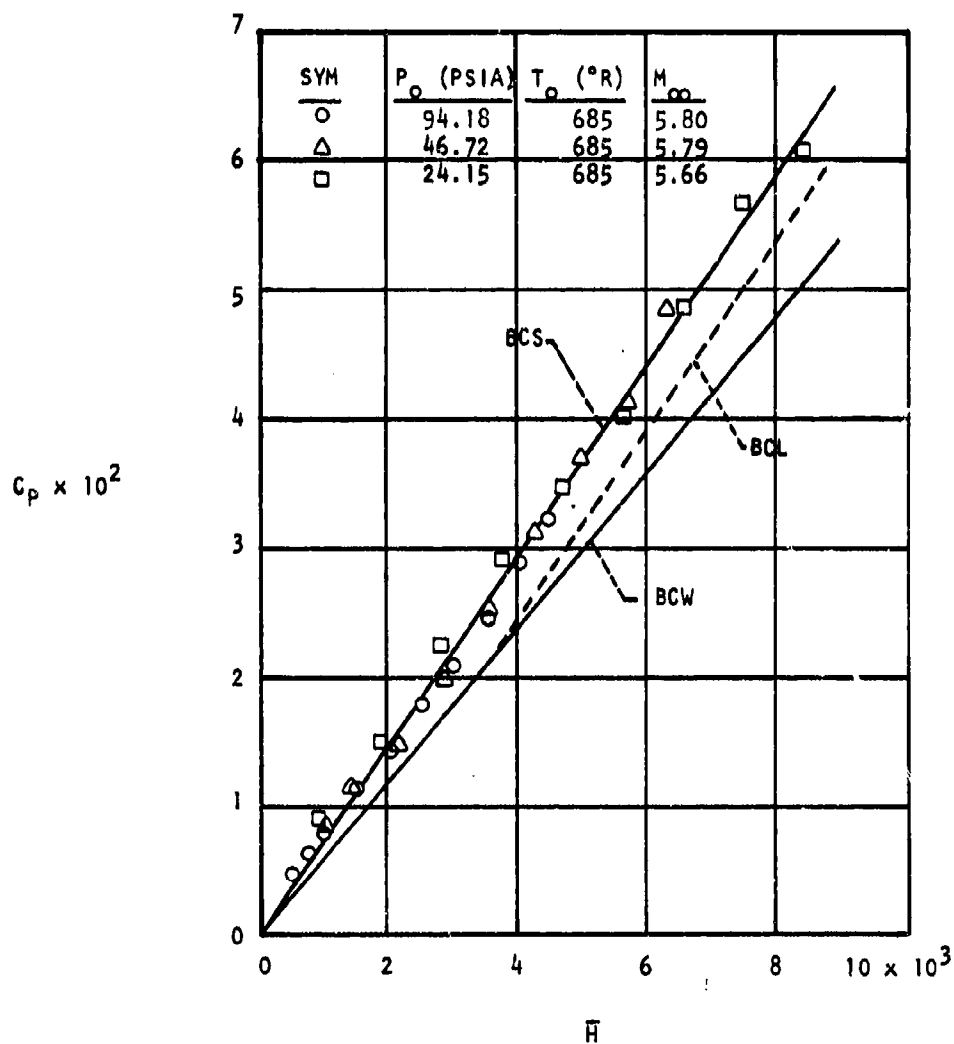
Figure 8. Comparison of Binary Collision Interaction
Theory with Experimental Pressure
Coefficient on Kendall's Flat Plate at
$\delta_{inv} = 0°$
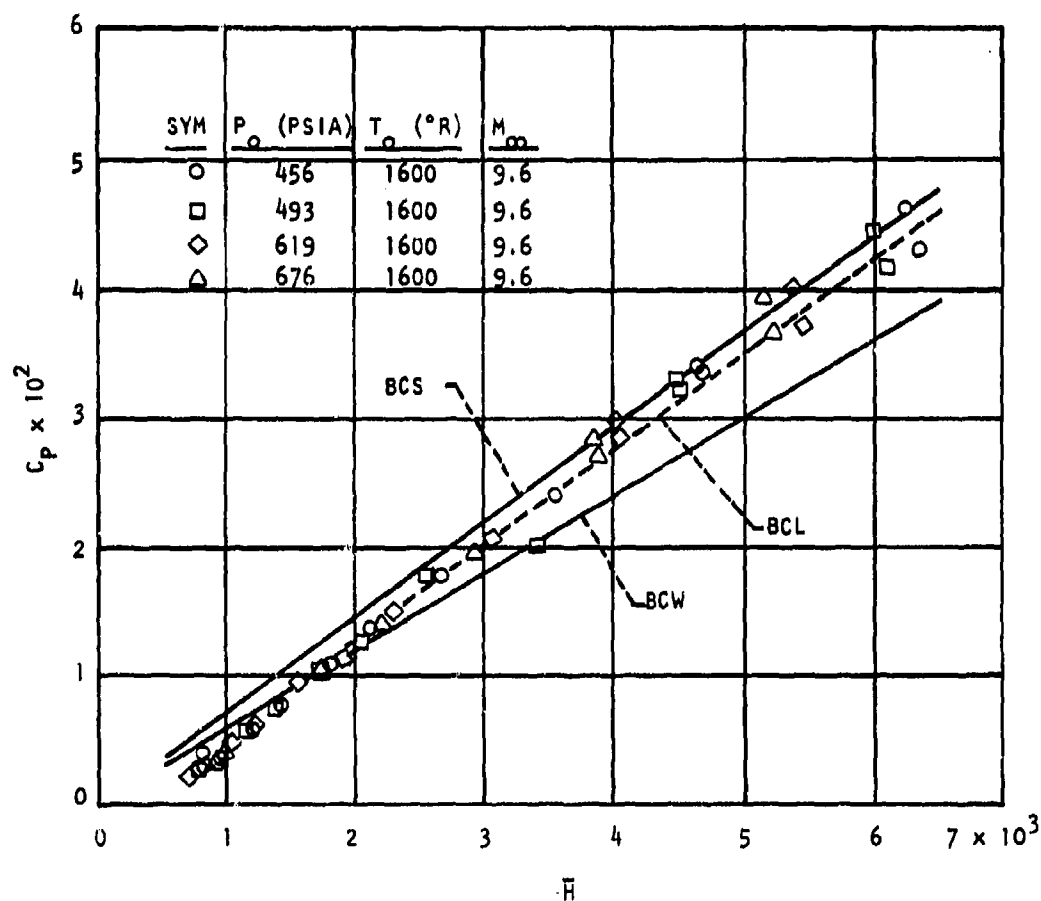
Figure 9. Comparison of Binary Collision Interaction
Theory with Experimental Pressure Coefficient
on Bertram's Flat Plate at $\delta_{inv} = 0°$

TABLE IV

CLASSICAL PREDICTIONS FOR $\left(M_\infty \dfrac{d\delta^*}{dx}\right)^2$

FOR FOUR TEST CASES

Test Case	Maximum				Minimum			
	$\dfrac{T_w}{T_o}$	$\bar{X}$	$\left(M_\infty \dfrac{d\delta^*}{dx}\right)^2$		$\dfrac{T_w}{T_o}$	$\bar{X}$	$\left(M_\infty \dfrac{d\delta^*}{dx}\right)^2$	
			Weak Interaction Equation 30	Strong Interaction Equation 31			Weak Interaction Equation 30	Strong Interaction Equation 31
AFFDL (p_0 = 200 psia)	.299	9.4	1.261	1.364	.299	4.2	.253	.611
AFFDL (p_0 = 500 psia)	.289	6.3	.550	.904	.289	2.8	.1086	.402
Kendall (M_∞ = 5.66)	.863	3.2	.579	.849	.863	.35	.0069	.0929
Bertram (M_∞ = 9.6)	.602	9.6	2.77	2.015	.407	1.45	.0409	.244

TABLE V

BINARY COLLISION PREDICTIONS AND EXPERIMENTAL VALUES FOR $\left(M_\infty \frac{d\delta^*}{dx}\right)^2$

FOR FOUR TEST CASES

Test Case	Maximum $\left(M_\infty \frac{d\delta^*}{dx}\right)^2$			Minimum $\left(M_\infty \frac{d\delta^*}{dx}\right)^2$		
	Binary Collision Weak, eq. 33 $x/x^* = 1$	Binary Collision Strong, eq. 33 $x/x^* = 1.5$	Experiment	Binary Collision Weak, eq. 33 $x/x^* = 1$	Binary Collision Strong, Eq. 33 $x/x^* = 1.5$	Experiment
AFFDL($p_0 = 200$ psia)	.462	.694	.855	.145	.218	.268
AFFDL($p_0 = 500$ psia)	.264	.397	.535	.0482	.0723	.142
Kendall ($M_\infty = 5.66$)	.318	.477	.428	.0078	.0117	.0168
Bertram ($M_\infty = 9.6$)	.935	1.402	1.261	.0626	.0939	.0299

Similar linearizations in the binary collision analysis reduce errors
generated when the restriction set up in Equation 30 is violated. The
AFFDL data (Figure 3) at $p_0 = 500$ psia approaches the weak interaction
limit while Bertram's case (Figure 5) best approximates the strong
interaction limit. The rest of the data falls between the two interaction
regions although most of Kendall's data (Figure 4) corresponds to the
weak interaction region. For different cases having similar values of
$\left(M_\infty \frac{d\delta^*}{dx}\right)^2$, varying degrees of correlation between data and theory exist.
In Kendall's case, good agreement between weak interaction theory and the
data occurs for $\overline{X} \leq 2$ which corresponds to $\left(M_\infty \frac{d\delta^*}{dx}\right)^2 \leq 0.25$, whereas
no similar correlation is apparent for Bertram until $\left(M_\infty \frac{d\delta^*}{dx}\right)^2 \leq 0.05$,
and even then the agreement is not as good as with Kendall. However,
this is probably due to other reasons which are discussed further on.
No particularly good correlation between AFFDL data and the weak inter-
action theory exists, although correlation with the Eckert reference-
temperature-dependent theory is better than with the Crocco reference
temperature. In the region where weak interaction effects would be
expected to dominate $(\overline{X} \leq 4)$ the data is 6% to 7% higher than the
Eckert-based theory, and 7% to 9% higher than the Crocco based results.
Agreement between weak interaction theory and data is best when adia-
batic wall conditions prevail but deteriorates as $T_w/T_0 \rightarrow 0$.

When the strong interaction solution (Equation 16) is compared with
AFFDL and Kendall's results (Figures 3 and 4), excellent correlation
with experimental results is observed. When Bertram's data is considered
the data trend is linear and parallel to the theory although a signifi-
cant amount below it. In order for a linear pressure correlation to
exist, the expression for $M_\infty(d\delta^*/dx)$ must be far more complicated than
indicated in Equation 32. Since many approximations and series trun-
cations were made in the derivation of Equation 32 (Reference 16), it is
quite likely that in the intermediate region, where neither weak nor
strong interactions predominate, the expression for $M_\infty(d\delta^*/dx)$ is quite
complex. Bertram had other "unpublished" data (Reference 16, Figure
9-4) that correlates very well with the classical, first order, strong

31

interaction theory for an insulated flat plate. These data are repro-
duced in Figure 6. For all four sets of data it appears that a linear
pressure variation does exist and that Equation 16 will accurately pre-
dict the pressures in the weak, intermediate, and strong interaction
regions.

In Figure 7 the AFFDL data are compared with the binary collision
scaling theory. If the AFFDL data at $p_0 = 200$ psia is examined in
detail, it can be shown that an 11% error in $M_\infty \frac{d\delta^*}{dx}$ plus an additional
3.3% error due to the linear approximation for C_p occurs. If a 14.3%
correction to the binary collision theory is made, excellent correlation
between data and strong interaction theory results. In contrast, if
similar corrections are made to Kendall's and Bertram's results, worse
correlation occurs. Similar corrections to the classical, weak inter-
action theory would promote better agreement between data and theory,
while no improvement on classical, strong interaction theory could
possibly result. Although the ratio between experimental values for
$\left(M_\infty \frac{d\delta^*}{dx}\right)^2$ and $\left(M_\infty \frac{d\delta^*}{dx}\right)^2$ determined by classical, strong interaction
theory is relatively constant over a large range of p/p_∞, the same is
not true when the binary collision prediction (Equation 33) is ratioed
to experimental values. Clearly, the binary collision prediction for
$\left(M_\infty \frac{d\delta^*}{dx}\right)^2$ for the AFFDL tests does not follow the same trend as do
either the classical weak or strong interaction predictions. The
deviation from the trend indicates that the binary collision result for
$M_\infty \frac{d\delta^*}{dx}$ gives too low a prediction for the AFFDL tests. The reason
for the low prediction is due to the cool wall temperatures encountered
in the AFFDL tests as opposed to the higher temperatures associated with
Kendall's and Bertram's tests. Due to the inclusion of a reference
temperature in conjunction with a linear velocity profile assumption in
the determination of δ^*/θ in Equation II-18, a 1% error in T^*/T_e is
capable of producing a 6% error in the binary collision prediction for
C_p, whereas in the classical prediction a 1% error in T^*/T_e will cause
less than a 1/2% error in the p/p_∞ ratio. Reference 9 shows that
greater errors in T^* will occur when the wall is cooled than when it is
at adiabatic or near adiabatic conditons. Therefore, the poor correla-
tion between binary collision theory and AFFDL data is due to the strong

theoretical dependence upon reference temperature. The effect of a more accurate estimation for T^* would show up only in Equation II-28 and not in Equation 30, which is only a simplified approximation. Consequently, good correlation should not be expected between current binary collision theory and data obtained at other than adiabatic wall conditions.

In Figure 9 data from Bertram's experiments (Ref.26) is compared with theory. The data agree fairly well with the linearized departure from the strong interaction limit in the binary collision scaling theory. However, the poor correlation of the same data and classical interaction theory (Figure 5) should be kept in mind before any final decision regarding the apparent good correlation with binary collision predictions is made. If the source for this data (Reference 26) is examined, it is apparent that the pressure distribution in the direction of flow varied as much as 6-1/2% over a distance of 3 inches in the vicinity of the nozzle exit plane. It was in this region that the model test data were obtained. In addition, a pressure difference of as much as 5% can be observed over a cross model distance of only 1.2 in. Since Bertram's model was not cooled and data were taken at less than adiabatic wall conditions, the wall temperature was continuously increasing, so the pressure was also continuously increasing. Therefore, at a given instant the pressure being sensed at the transducer may not have been the same as that being experienced at the model surface due to unfavorable tubulation lag time characteristics. For these reasons, not as much creditability should be conferred on Bertram's data as on either Kendall's or the AFFDL data.

Before going on, some comment should be made with regard to Kendall's data. Although the results were published in 1957, the pressures measured were well within the instrumentation capabilities at that time. Little scatter and good repeatability may also be observed from his data. Although Kendall's pressure taps were located over a flat plate distance nearly identical to Bertram's, no flat plate side effects or other anomalies are discernable. The flat plate used by Kendall was allowed to reach the equilibrium temperature (adiabatic wall) before pressure measurements were made. Therefore, no pressure lag time effects would

be expected. Thus, one can have much more confidence in using Kendall's data.

2. FLAT PLATE INCLINED TO THE FREESTREAM $(\delta_{inv} > 0°)$

For $\delta_{inv} > 0°$, weak interaction effects predominate when $M_\infty \frac{d\delta^*}{dx}$ is less than or of the order of one or when $\frac{d\delta^*}{dx} < \delta_{inv}$ with $M_\infty \delta_{inv}$ arbitrary. This criteria was satisfied for all the AFFDL test cases.

A major difficulty encountered in evaluating the data at higher angles of attack was selection of the most representative data point. Although the HTF is essentially a steady state wind tunnel, a very small amount of flow field fluctuation, on the order of $\pm$ 1% in p_∞ occurred, which caused the reduced data to vary in such a manner that, for $\delta_{inv} \gtrsim 10°$, data from at least one test point from each run fell on or between the weak and strong binary collision solutions. It was this test point which was chosen to be representative of all the data obtained on that particular run.

The measurements of surface pressures on a wedge at 5, 10, and 15 degrees angles of attack are shown in Figures 10 through 15. It can be seen that the second order, weak interaction theory agrees quite well with the experimental surface pressure on the wedge for all three angles of attack. Agreement between data and classical weak interaction theory can be improved slightly if the Eckert reference temperature is used in the calculation of d_{orig}. Results using Eckert's reference temperature afford approximately a 1% increase in the theoretical pressure estimate. At $\delta_{inv} = 5.11°$, the exact solution to the binary collision theory suffers some of the nonlinear effects mentioned in Appendix III. At the two higher angles (10° and 15°), the weak limit to the binary collision solution provides reasonably good correlation with data. Moreover, the classical weak and binary collision weak solutions agree remarkably well with each other for the three angles of attack shown.

Figure 10. Comparison of Classical Interaction Theory with Experimental Pressure Distribution on the AFFDL Flat Plate at $\delta_{inv} = 5.11°$

Figure 11. Comparison of Binary Collision Interaction Theory
with Experimental Pressure Coefficient on the
AFFDL Flat Plate at $\delta_{1nv} = 5.11°$

Figure 12.   Comparison of Classical Interaction Theory with Experimental Pressure Distribution on the AFFDL Flat Plate at $\delta_{inv} = 10.12°$

Figure 13. Comparison of Binary Collision Interaction Theory with Experimental Pressure Coefficient on the AFFDL Flat Plate at $\delta_{inv} = 10.12°$
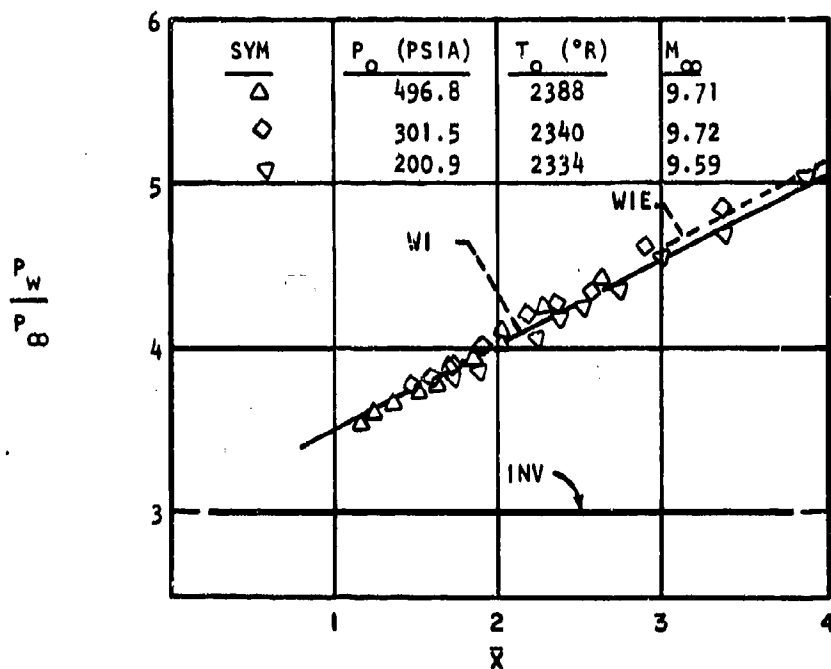
Figure 14. Comparison of Classical Interaction Theory with Experimental Pressure Distribution on the AFFDL Flat Plate at δ_{inv} = 15.21°
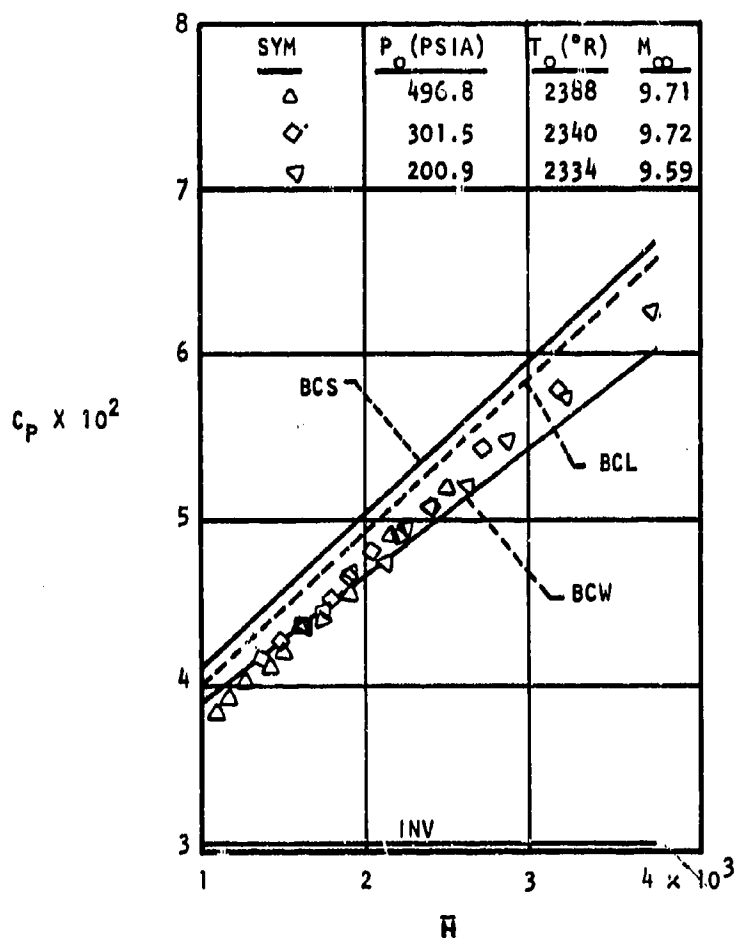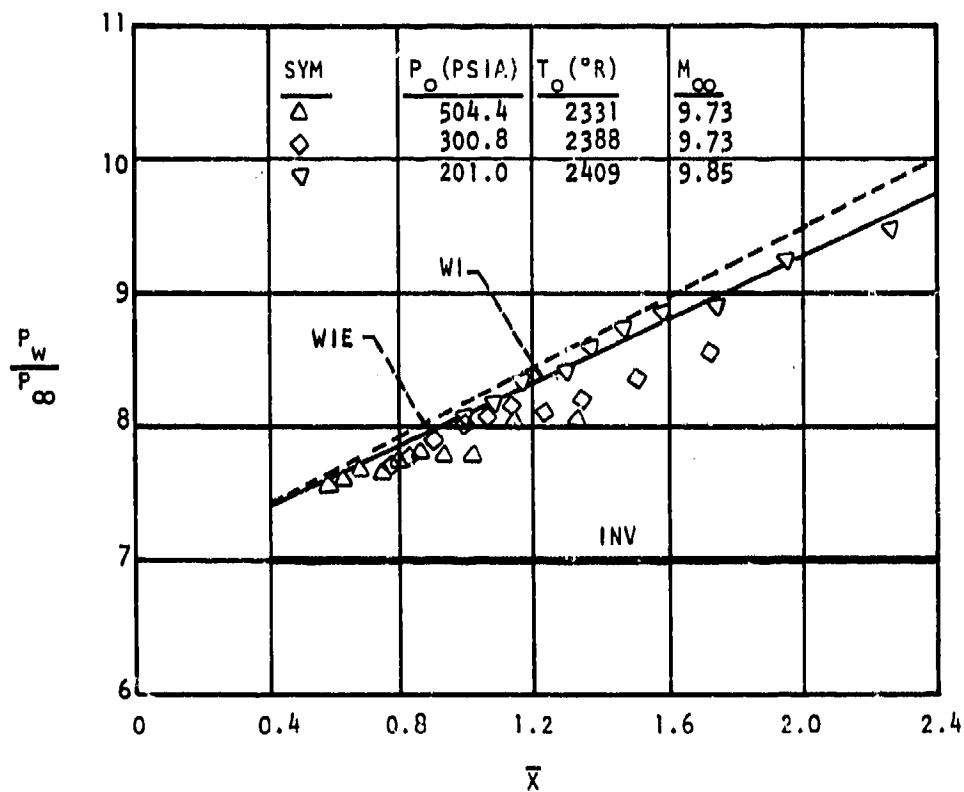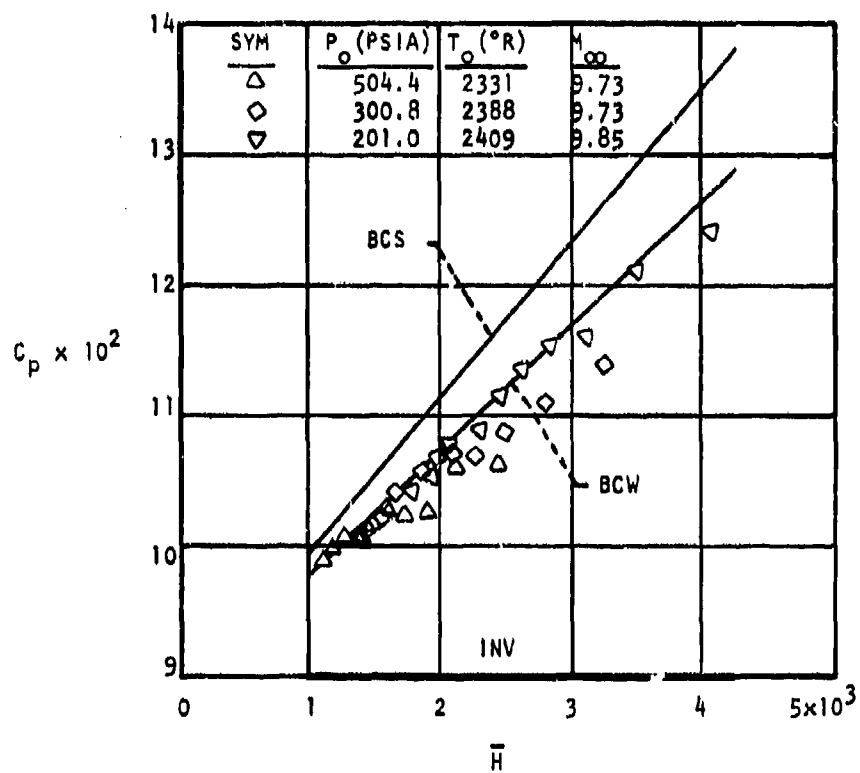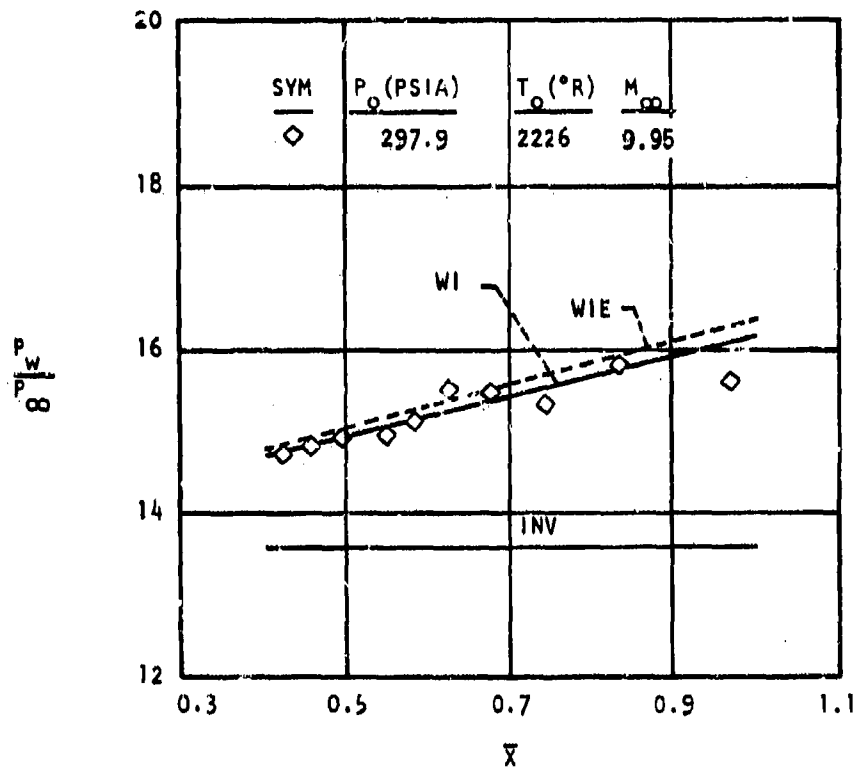
Figure 15. Comparison of Binary Collision Interaction Theory with Experimental Pressure Coefficient on the AFFDL Flat Plate at δ_{inv} = 15.21°

40

As the angle of attack is increased, the linearized binary collision theory increases to the point where the results are indistinguishable from the strong interaction limit values. This result is due to the very large value for p/p_∞ which forces the second term on the right hand side of Equation 21 toward zero.

The test run at $p_0 = 200$ psia and $\delta_{inv} = 15°$ did not last long enough for the model pressures to reach equilibrium conditions. Consequently, the data from this run is not included in this report. In addition the $\delta_{inv} = 16°$ case was inadvertently never run.

Data at $\delta_{inv} = 15°$ and $p_0 = 500$ psia were also obtained, but the thermocouple output saturated the analog-to-digital equipment and an accurate wall temperature was not obtained. However, the very pronounced and abrupt departure of data from the straight line prediction at this condition is considered important enough to be included in this report and is shown in Figures 16 and 17.

Originally, it was planned that data would be taken at $p_0 = 200, 300,$ and 500 psia, and $\delta_{inv} = 5°, 10°$ and $15°$. However, the unusual pressure dip near the leading edge at $p_0 = 500$ psia and $\delta_{inv} = 15°$ warranted additional exploration at angles of attack in the vicinity of 15°. These additional tests were made at $p_0 = 500$ psia only due to limited test time. Results for $p_0 = 500$ psia and $\delta_{inv} = 11°, 12°, 13°, 14°, 17°, 19°$ and $20°$ are shown in Figures 18 through 31.

Near the leading edge the experimental pressures are lower than the predicted values. The degree of departure is most evident in the vicinity of $\delta_{inv} = 15°$, when the freestream unit Reynolds number is 4.15×10^5. When the Reynolds number is decreased, the effect is less pronounced. No departure is evident at $\delta_{inv} = 5°$, but some nonlinear effects are still noticeable at $\delta_{inv} = 20°$.

Figure 16. Comparison of Classical Interaction Theory with Experimental Pressure Distribution on the AFFDL Flat Plate at $\delta_{inv} = 15.28°$
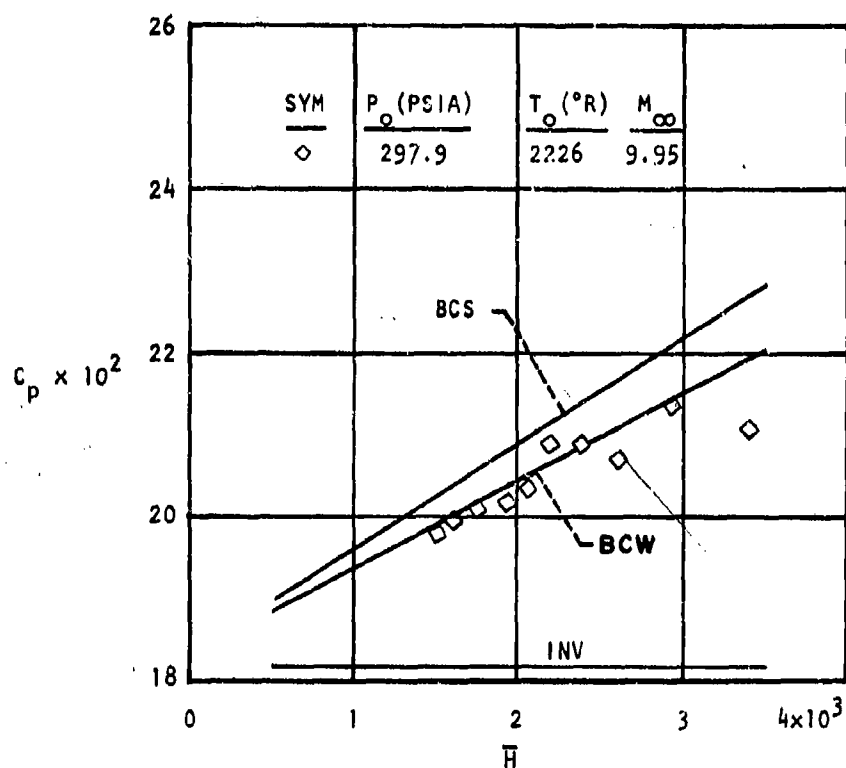
Figure 17. Comparison of Binary Collision Interaction Theory
with Experimental Pressure Coefficient on the
AFFDL Flat Plate at $\delta_{inv} = 15.28°$

Figure 18. Comparison of Classical Interaction Theory
with Experimental Pressure Distribution on
the AFFDL Flat Plate at $\delta_{inv} = 11.19°$

Figure 19. Comparison of Binary Collision Interaction Theory with Experimental Pressure Coefficient on the AFFDL Flat Plate at $\delta_{inv} = 11.19°$

Figure 20. Comparison of Classical Interaction Theory
with Experimental Pressure Distribution on the
AFFDL Flat Plate at δ_{1nv} = 12.23°

Figure 21. Comparison of Binary Collision Interaction Theory
with Experimental Pressure Coefficient on the
AFFDL Flat Plate at δ_{inv} = 12.23°
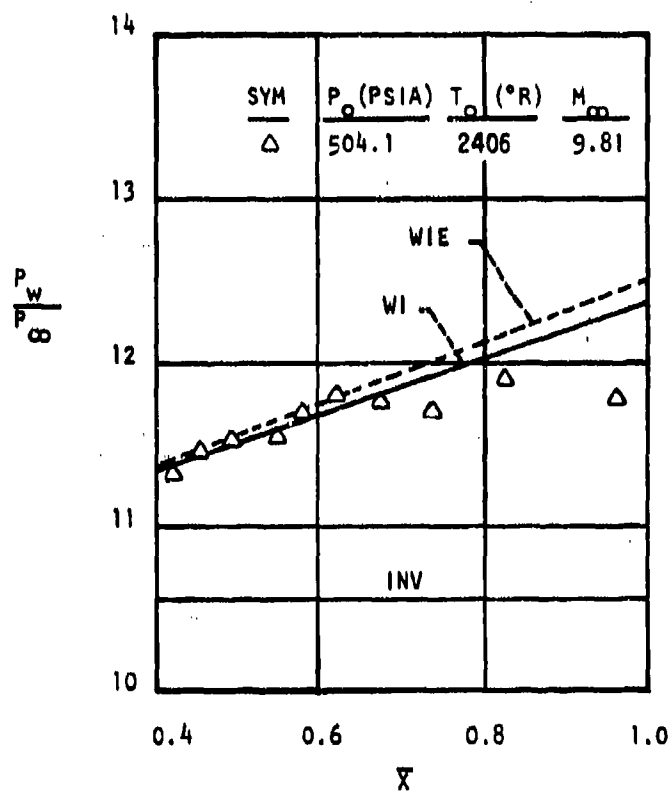
Figure 22. Comparison of Classical Interaction Theory with Experimental Pressure Distribution on the AFFDL Flat Plate at δ_{inv} = 13.21°
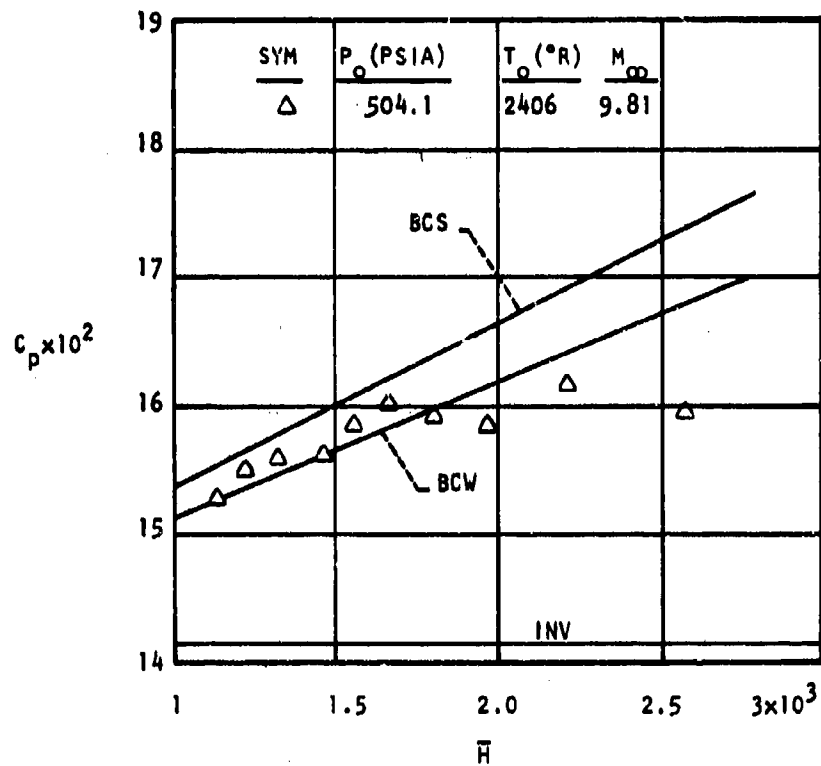
Figure 23. Comparison of Binary Collision Interaction Theory with Experimental Pressure Coefficient on the AFFDL Flat Plate at $\delta_{inv} = 13.21°$
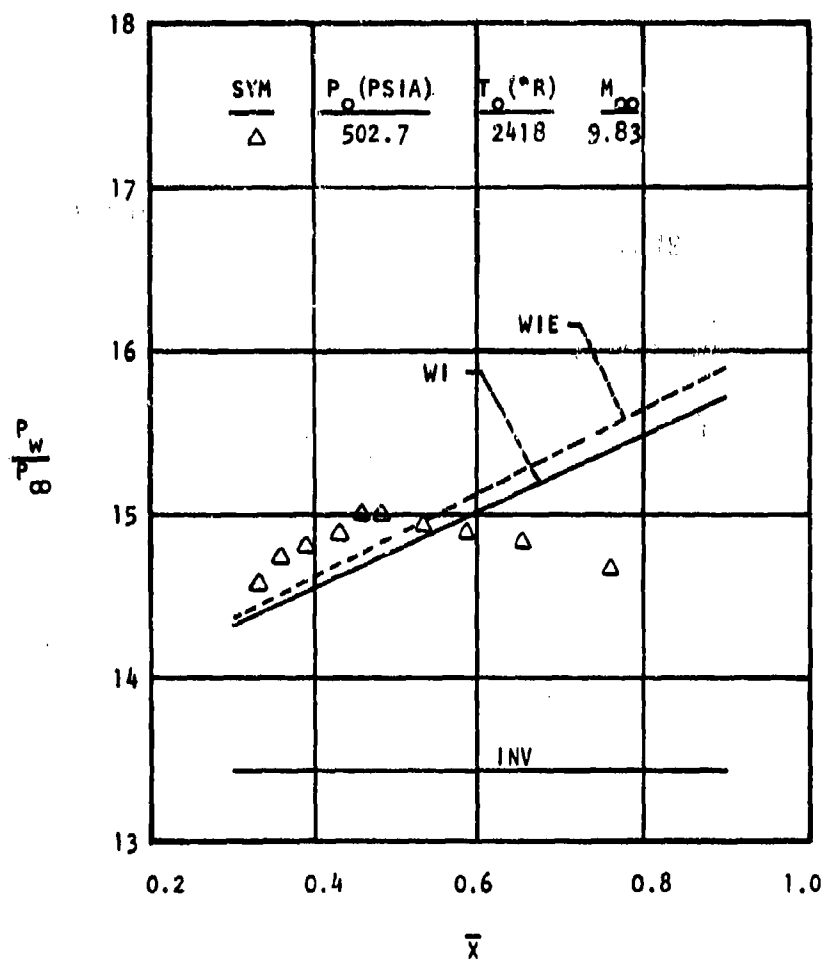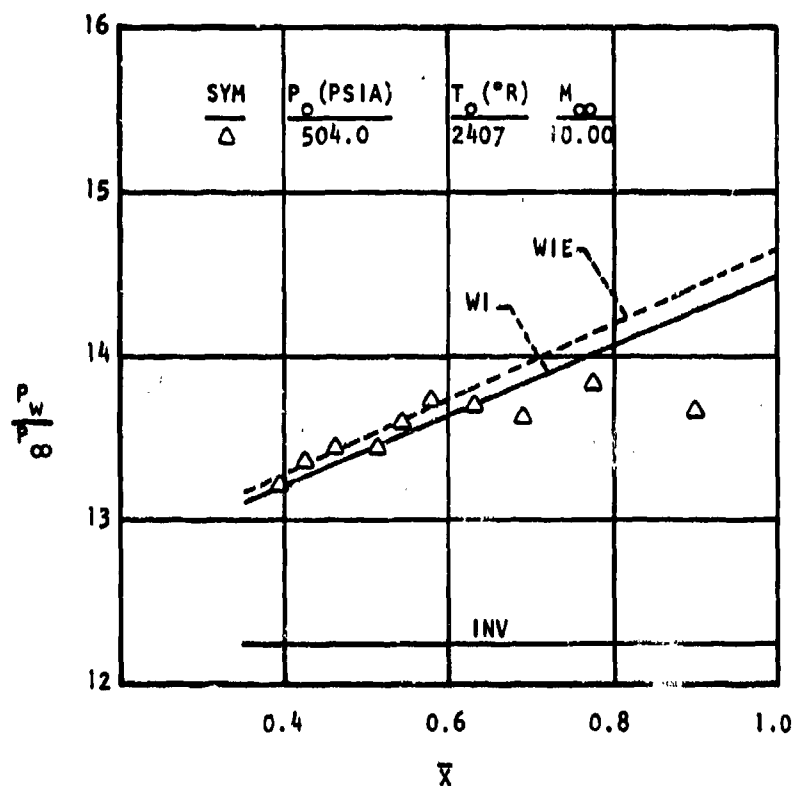
Figure 24. Comparison of Classical Interaction Theory with Experimental Pressure Distribution on the AFFDL Flat Plate at δ_{inv} 14.20°
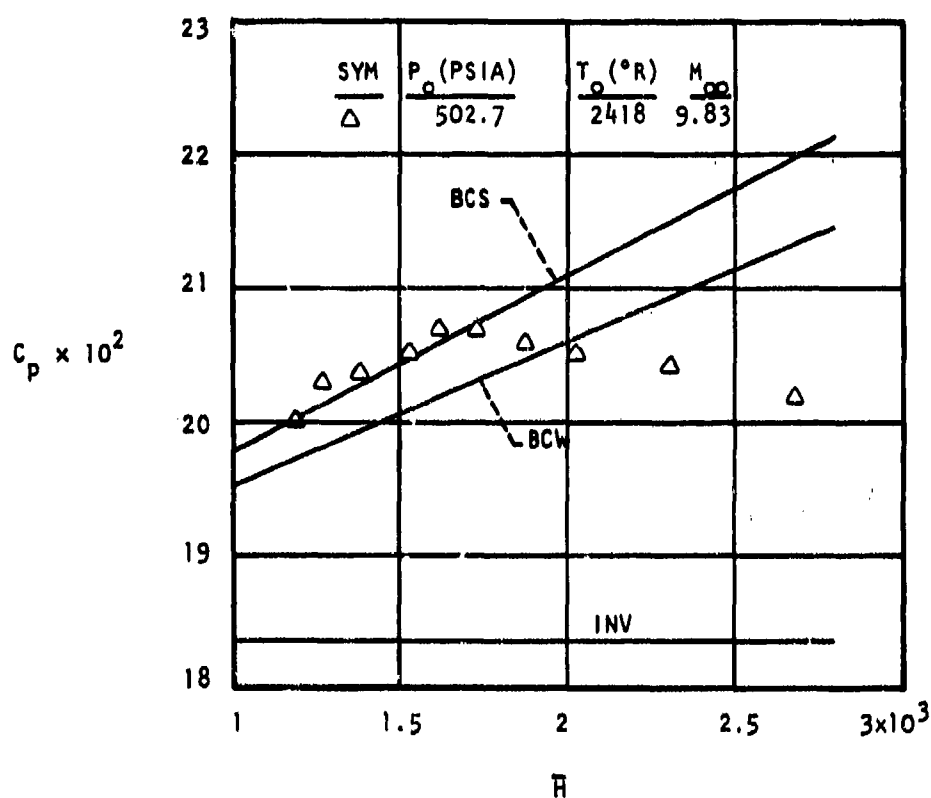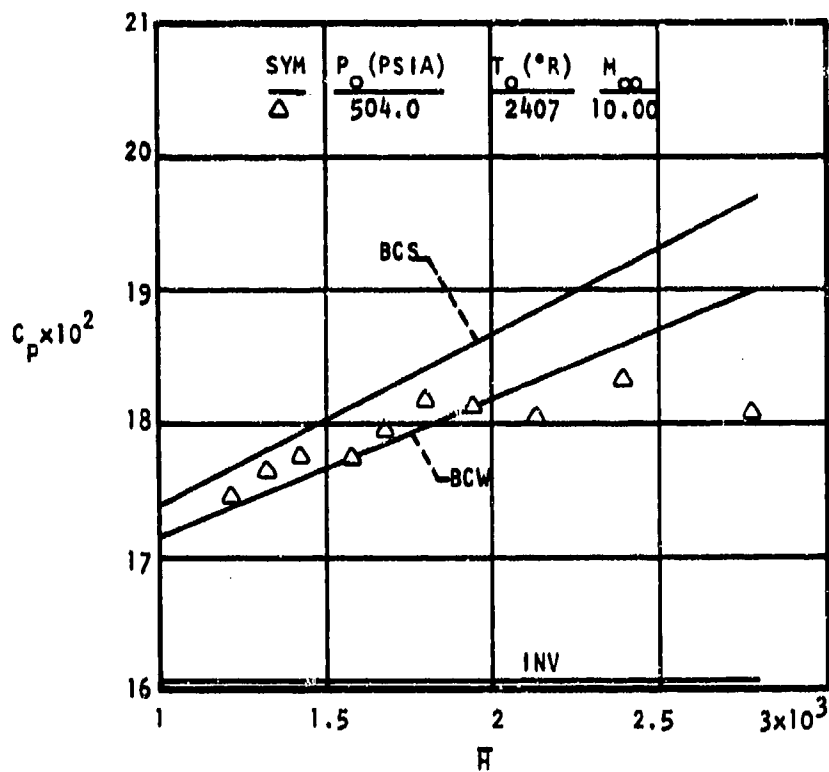
Figure 25. Comparison of Binary Collision Interaction Theory
with Experimental Pressure Coefficient on the
AFFDL Flat Plate at $\delta_{inv} = 14.20°$
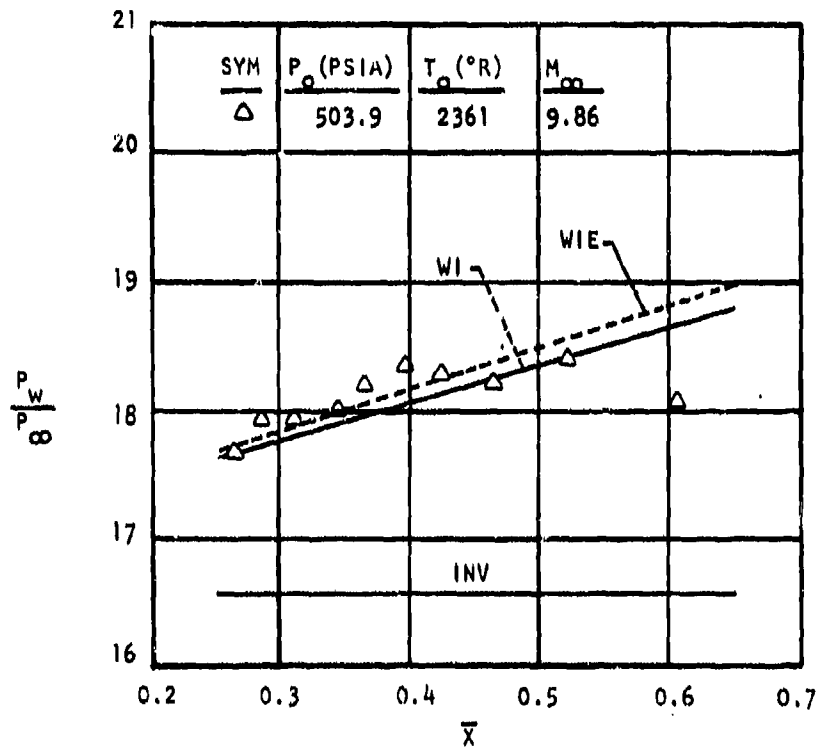
Figure 26. Comparison of Classical Interaction Theory with
Experimental Pressure Distribution on the AFFDL
Flat Plate at δ_{inv} = 17.25°

$c_p \times 10^2$

Figure 27. Comparison of Binary Collision Interaction
Theory with Experimental Pressure Coefficient
on the AFFDL Flat Plate at $\delta_{inv} = 17.25°$

53
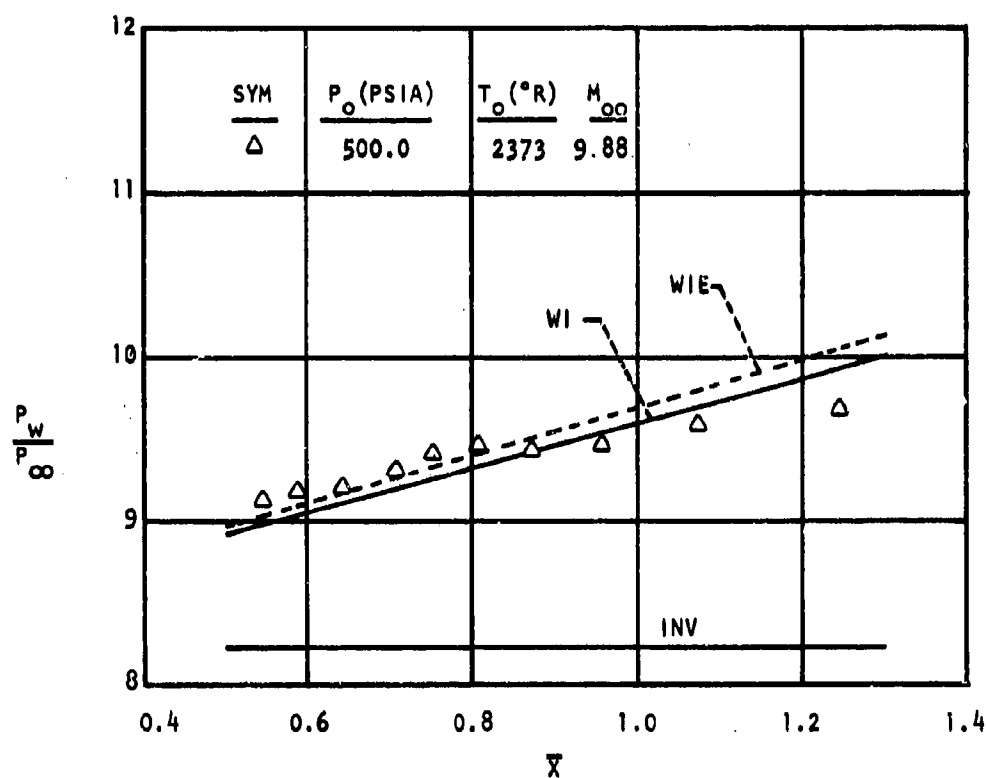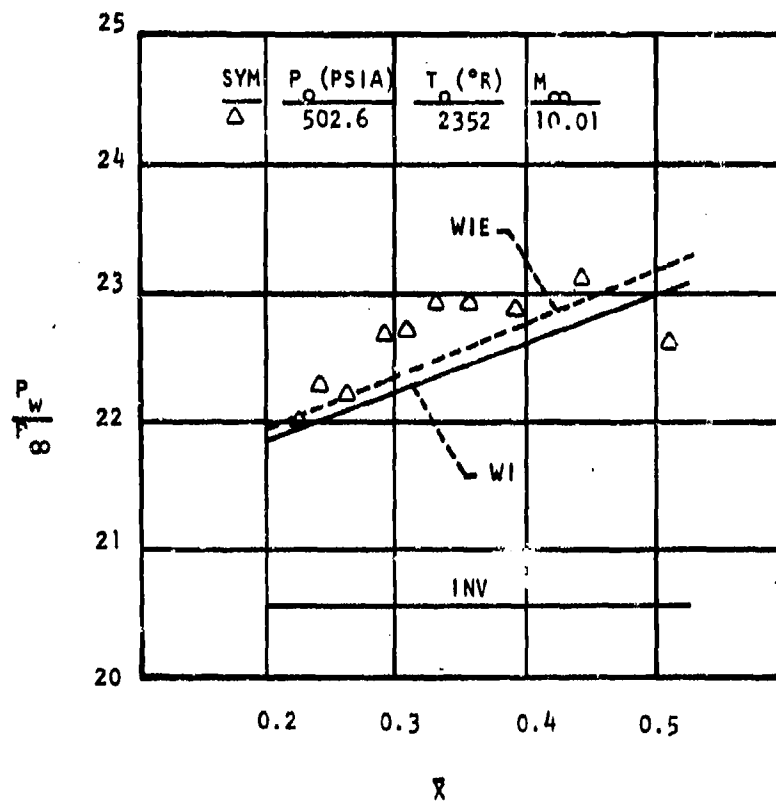
Figure 28. Comparison of Classical Interaction Theory with
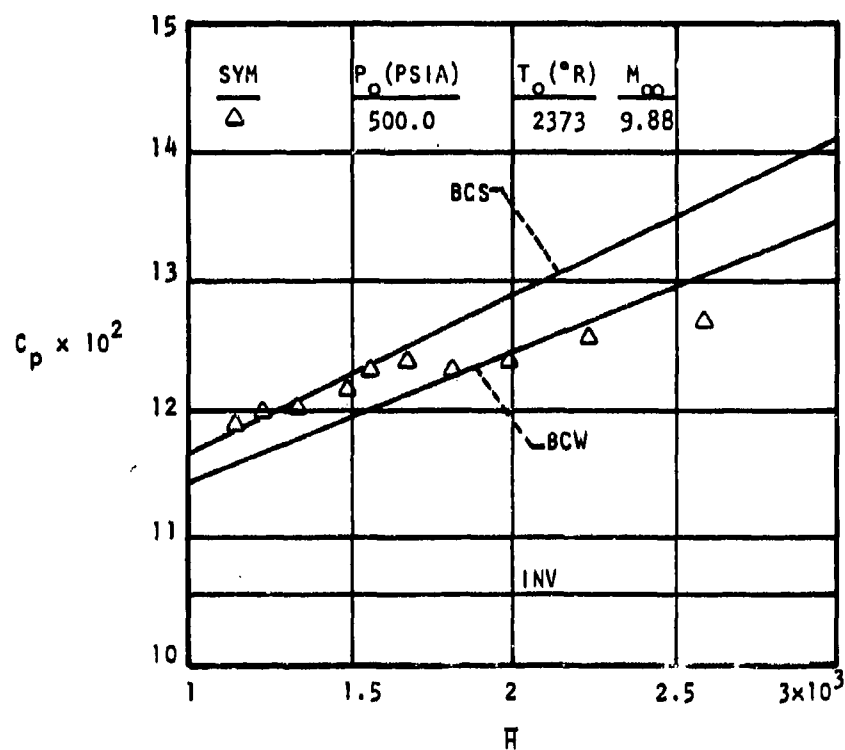Experimental Pressure Distribution on the AFFDL
Flat Plate at δ_{inv} = 19.24°

Figure 29. Comparison of Binary Collision Interaction Theory
with Experimental Pressure Coefficient on the
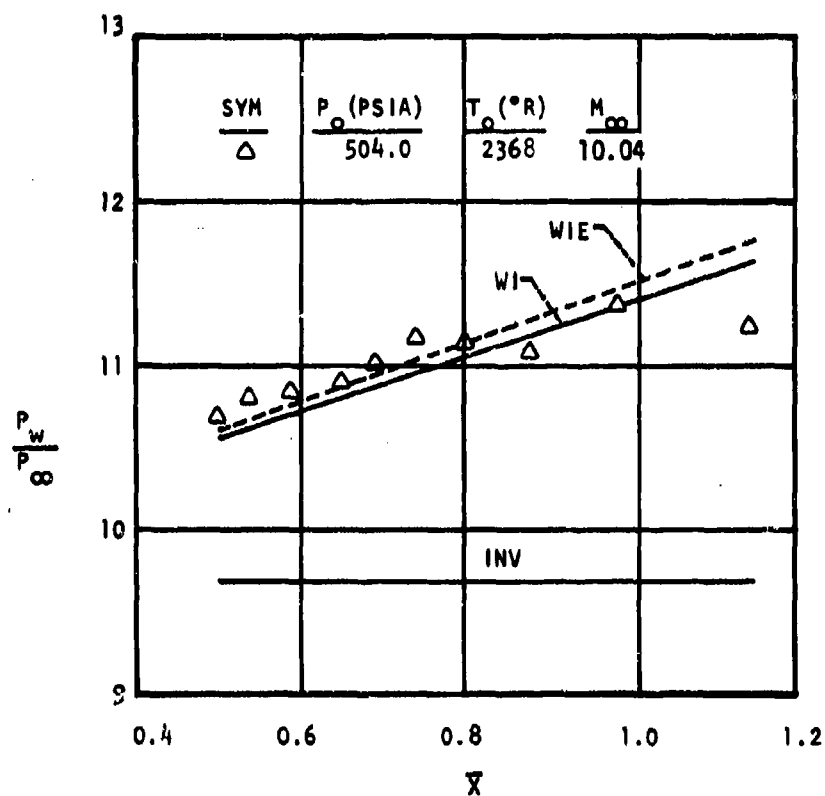AFFDL Flat Plate at $\delta_{inv} \approx 19.24°$
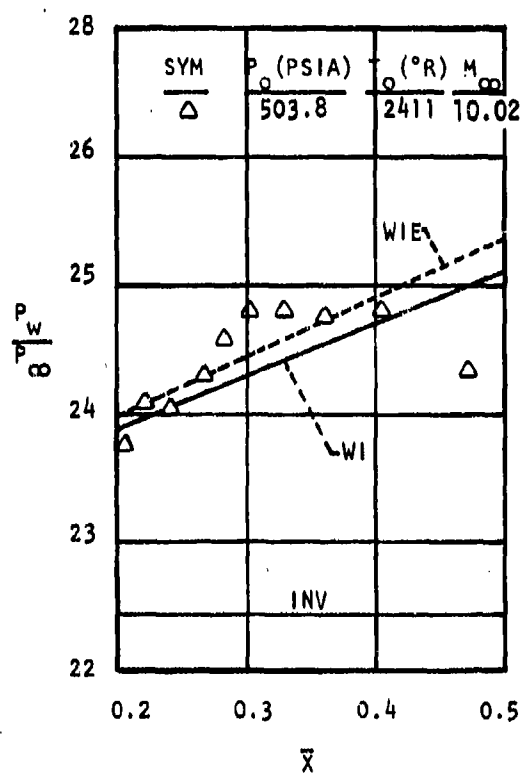
Figure 30. Comparison of Classical Interaction Theory with
Experimental Pressure Distribution on the AFFDL
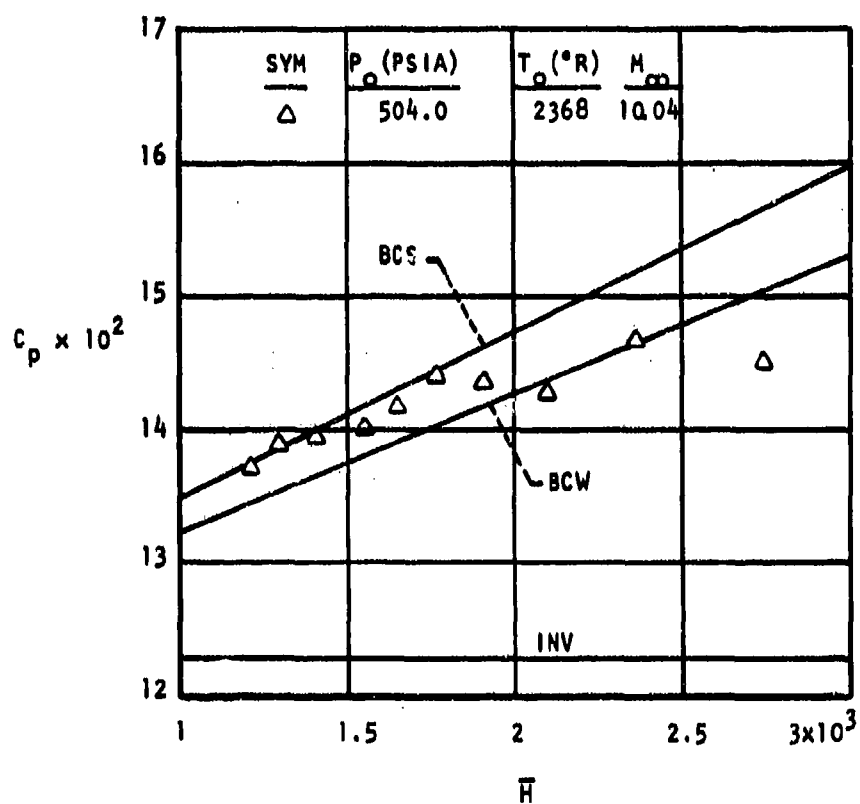Flat Plate at $\delta_{inv} = 20.20°$
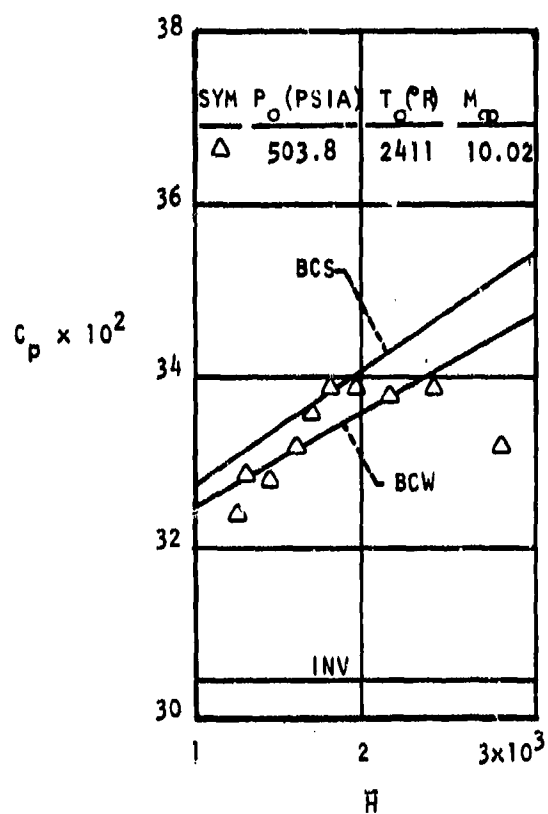
Figure 31. Comparison of Binary Collision Interaction Theory with Experimental Pressure Coefficient on the AFFDL Flat Plate at $\delta_{inv} = 20.20°$
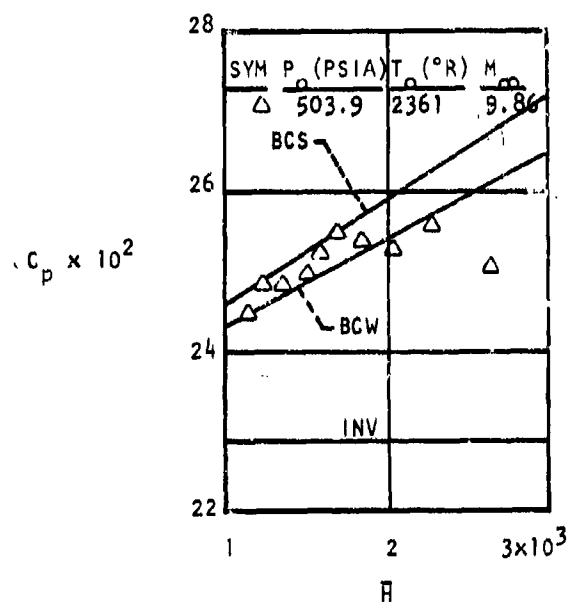
Other experimenters (Reference 27, 28, 29, and 30) have attributed
this pressure fall-off near the leading edge to merging of the boundary
layer and shock wave. In the present tests, there is some question as
to whether the pressure decrease is due to merging or to some other
unknown phenomena, since the effect becomes more pronounced with increas-
ing freestream unit Reynolds number. This is contrary to the usual flat
plate explanation based on the onset of the merged layer regime (References
27 and 28) and contrary to the experimental results presented in References
29 and 30.

In Reference 27 tests on a sharp flat plate showed that the onset
of merging began at about $\overline{V}_\infty = 0.15$. However, this limit is based on
the zero degree angle of attack situation. Pan and Probstein (Reference
28) estimated the pressure deviations in the merged region with respect
to a zeroth order, strong interaction equation. Again, however, the
calculations are only for a flat plate at zero degrees angle of attack
and for a Mach number on the order of ten or greater.

Vas, Iacavazzi, Carlomagno and Bogdonoff (Reference 29) investigated
experimentally the effect of angle of attack on pressure distributions
on and near the merged regime for sharp leading edge wedges. They were
not able to correlate the merged region length with a $\overline{V}$ based on either
freestream or local inviscid wedge conditions. For $M_\infty = 25$, $Tw/T_0 = .15$
and $Re_\infty/IN = 9300$ the onset of merging occurred in the vicinity of
$\overline{V}_\infty = 0.17$ at $\delta_{inv} = 5°$ while at $\delta_{inv} = 14°$ merging began when $\overline{V}_\infty \geq .21$.

The experiments of McCrosky, Bogdonoff, and Genchi (Reference 30)
indicate that the onset of merging at angle of attack is not a simple
function of $\overline{V}_\infty$, and that merging occurred at between one to two inches
for $\delta_{inv} = 8°$ and at about one inch for $\delta_{inv} = 15°$. This result is not
in agreement with the trend of the AFFDL results for $P_0 = 500$ psia where
merging becomes evident at about one inch at $\delta_{inv} = 10°$ and at about
1.2 inch at $\delta_{inv} = 15°$. However, identification of the point of depart-
ure from an interaction type solution is somewhat arbitrary and, in the
present case, difficult.

Harney and Petrie (Reference 22, Figure 4) encountered merging effects in experiments made in argon-air mixtures. Merging effects became noticeable at all angles of attack when $\bar{H}$ reached a value of 6000 to 8000.

Present AFFDL results begin to deviate from interaction predictions for values of $\bar{H}$ as low as 2000 (Figure 17) and $\bar{V}_e$ as low as 0.022. No correlation between the data and $\bar{V}$ based on either freestream or local inviscid wedge conditions exists. Clearly, the present results show that significant deviations from the strong interaction prediction occur for values of $\bar{H}$ and $\bar{V}$ considerably smaller than that encountered in other similar tests (References 22, 29, and 30) for compression angles of attack.

At present no theory exists that can correlate pressure data on flat plates at angle of attack when merging effects are present.

SECTION VI

CONCLUSIONS

Detailed experimental pressures were generated on a flat plate both at zero and compression angles of attack in a hypersonic flow field. Pressure data are compared with several interaction theories and with data taken in other wind tunnel facilities.

At $\delta_{inv} = 0°$ the classical strong interaction theory agrees with the AFFDL data taken under cool wall conditions much better than either the classical weak or binary collision predictions. The poor correlation between data and binary collision theory is attributable to the cool wall conditions that existed during the tests.

At all angles of attack it is shown that the classical weak interaction theory can be improved slightly if Eckert's reference temperature is used in place of Crocco's.

At angle of attack both the classical and binary collision weak interaction solutions correlate very well with data except for a pressure dip near the leading edge at angles of attack at and in the vicinity of 15°. It is thought that this dip is due to the merging of the boundary layer, although values for the rarefaction parameter do not satisfy the usual conditions necessary for the onset of merging.

APPENDIX I

DETAILS OF CALCULATIONS FOR THE PRANDTL NUMBER, REFERENCE
TEMPERATURE, AND CHAPMAN-RUBESIN VISCOSITY-TEMPERATURE RELATION

1. PRANDTL NUMBER, P_r

A least square curve fit of data presented in Reference 32 is used to determine the Prandtl number,

$$P_r = A + B T + C T^2 , \qquad (I-1)$$

where

$200°R \leq T \leq 1000°R$

$A = .8238997$

$B = -.2975599 \times 10^{-3}$

$C = .1522722 \times 10^{-6}$

and

$1000°R < T \leq 1800°R$

$A = .6772683$

$B = -.145707 \times 10^{-4}$

$C = .1579909 \times 10^{-7}$

2. REFERENCE TEMPERATURE, T^*

Following Eckert (Reference 9) the relation for T^* is

$$T^* = T_e + .5(T_w - T_e) + .22 (T_{aw} - T_e) \qquad (I-2)$$

To find the adiabatic wall temperature

$$T_{aw} = T_e + r^* (T_o - T_e) \qquad (I-3)$$

it is necessary to evaluate the recovery factor, r^*, which for a laminar boundary layer is

$$r^* = \sqrt{P_r^*} \qquad (I-4)$$

Finally, an expression for T* is obtained

$$T^* = .5(T_e + T_w) + .22 \sqrt{P_r^*} (T_0 - T_e) \qquad (I-5)$$

Since the P_r - T approximation is limited to a second order curve fit, it is possible to solve for T* explicitly.

$$T^* = \left(\sqrt{B^2 - 4AC} - B \right) \Big/ 2A \qquad (I-6)$$

For $1000°R < T^* \leq 1800°R$

$$A = 1 - 7.6467498 (T_0 - T_e)^2 \times 10^{-8}$$

$$B = 7.0522188 (T_0 - T_e)^2 \times 10^{-7} - (T_e + T_w)$$

$$C = .25 (T_e + T_w)^2 - 3.2779785 (T_0 - T_e)^2 \times 10^{-2}$$

For $200°R \leq T^* \leq 1000°R$

$$A = 1 - 7.3699744 (T_0 - T_e)^2 \times 10^{-9}$$

$$B = 1.4401899 (T_0 - T_e)^2 \times 10^{-5} - (T_e + T_w)$$

$$C = .25 (T_e + T_w) - 3.9876745 (T_0 - T_e)^2 \times 10^{-2}$$

3. CHAPMAN - RUBESIN RATIO, C*

When T* is known, it is a simple matter to calculate the reference viscosity, μ^* by using either the Hirschfelder (Reference 33) or Sutherland Equations.

For $T^* < 200°R$

$$\mu^* = 8.051 \, T^* \times 10^{-10} \left(\frac{LB - SEC}{FT^2} \right) \qquad (I-7)$$

63

For $T^* \geq 200°R$

$$\mu^* = 2.27 \frac{T^{*3/2}}{T^* + 198.6} \times 10^{-8} \left(\frac{LB - SEC}{FT^2} \right) \qquad (I-8)$$

By incorporating the usual approximation that the pressure is constant across the boundary layer, the Chapman-Rubesin ratio,

$$C^* = \frac{\rho^* \mu^*}{\rho_e \mu_e} \qquad (I-9)$$

becomes

$$C^* = \frac{T_e \mu^*}{T^* \mu_e} \qquad (I-10)$$

4. ECKERT REFERENCE TEMPERATURE RELATION FOR d_{orig}

The Eckert reference temperature can be used in conjunction with the zero pressure gradient result for boundary layer displacement thickness growth,

$$\delta^* = 1.7208 x / \sqrt{Re^*_{\infty_x}} \qquad (I-11)$$

to obtain

$$\delta^* \sqrt{\frac{1}{X} \frac{\rho_e u_e}{\mu_e C^*}} = 1.7208 \left(\frac{T^*}{T_e} \right) \qquad (I-12)$$

After differentiating this expression to find $d\delta^*/dx$, Equation I-2 is used to get

$$\frac{d\delta^*}{dx} = \frac{X}{M_e} d_{orig} \qquad (I-13)$$

where

$$d_{orig} = .4302 \left[\frac{1 + \frac{T_w}{T_o}}{M_e^2} + (\gamma - 1) \left(.44 \sqrt{Pr^*} + \frac{T_w}{T_o} \right) \right] . \qquad (I-14)$$

64

APPENDIX II

A SUMMARY OF THE HYPERSONIC VISCOUS INTERACTION PHENOMENA IN
TERMS OF HARNEY'S BINARY COLLISION SCALING PARAMETER, $(\rho_\infty x^*)^{-1/2}$

The analysis contained in this appendix is entirely attributable to
Dr. D. J. Harney of the AFFDL and is presented here for the convenience
of the reader. Because it circumvents the need to have an accurate free-
stream Mach number, as is required in classical theory, it is most valu-
able in connection with experiments in very high energy wind tunnels
where non-equilibrium effects become significant and Mach number deter-
mination is uncertain. It is included in this report because there is
no good reason why the theory should not be applicable to tests conducted
in equilibrium flow fields. The method can be simply stated as follows:
The pressure coefficient, Cp, can be represented as a function of the
gas properties, the freestream flow conditions, and the effective angle
of attack of the body. The effective angle of attack is the sum of the
geometric angle of attack plus the added body thickness caused by the
displacement effect of the viscous boundary layer as it exists in the
viscous interaction region. The hypersonic, small disturbance, tangent-
wedge theory due to Linnell (Reference 34) is used to account for the
inviscid processes, while the compressible, laminar boundary layer effects
are accounted for by a reference property transformation of Blasius'
incompressible flat plate boundary layer equations. The pressure grad-
ient resulting from the interaction effect is accounted for by a suitable
transformation of the streamwise coordinate. This analysis, attributable
to Harney (Reference 20) is described here.

1. INVISCID EFFECTS

For planar flow the small disturbance, tangent-wedge theory of
Linnell (Reference 35) is

$$\frac{C_p}{\sin^2 \delta} = \frac{\gamma + 1}{2} + \sqrt{\left(\frac{\gamma + 1}{2}\right)^2 + \left(\frac{2}{M_\infty \sin \delta}\right)^2} , \qquad (II-1)$$

where in our case δ is the sum of the geometric angle of attack plus the
viscous induced angle of attack attributable to boundary layer displace-
ment effects.

$$\delta = \delta_{inv} + \frac{d\delta^*}{dx} . \qquad (II-2)$$

Within the realm of small disturbance theory it is also assumed that $M_\infty \sin\delta \gg 1$, so that

$$\sqrt{\left(\frac{\gamma+1}{2}\right)^2 + \left(\frac{2}{M_\infty \sin\delta}\right)^2} = \frac{\gamma+1}{2} + \frac{1}{2}\left(\frac{2}{M_\infty \sin\delta}\right)^2 \bigg/ \left(\frac{\gamma+1}{2}\right) + \cdots \quad (II-3)$$

By substituting the first two terms of the binomial expansion given above into the small disturbance equation, the following result (Reference 31, Equation 5) is arrived at:

$$\frac{C_p}{\sin^2\delta} = (\gamma+1) + \frac{4}{(\gamma+1) M_\infty^2 \sin^2\delta} \quad . \quad (II-4)$$

Using the usual perfect gas relationship for M_∞,

$$\frac{1}{2} \rho_\infty u_\infty^2 = q_\infty = \frac{1}{2} \gamma p_\infty M_\infty^2 , \quad (II-5)$$

the pressure coefficient expression reduces to

$$\frac{C_p}{\sin^2\delta} = (\gamma+1) + \frac{2\gamma}{\gamma+1} \frac{p_\infty}{q_\infty \sin^2\delta} \quad (II-6)$$

Because the second term of this expression is much less than the first, the effect of γ is contained primarily in the first term.

The coefficient

$$\frac{2\gamma}{\gamma+1} \quad (II-7)$$

may then be considered a constant, b.

$$\frac{C_p}{\sin^2\delta} = (\gamma+1) + \frac{bp_\infty}{q_\infty \sin^2\delta} \quad (II-8)$$

or, rewriting

$$\frac{p - (1+b) p_\infty}{q_\infty} = (\gamma+1) \sin^2\delta \quad (II-9)$$

Harney (Reference 31) defined the left hand side of this equation as $C_p^{\sim}$

$$C_p' = (\gamma + 1) \sin^2 \delta \qquad (II-10)$$

or, in terms of C_p,

$$C_p = C_p' + \frac{b p_\infty}{q_\infty} = C_p' + \frac{2b}{\gamma M_\infty^2} \cdot \qquad (II-11)$$

The best justification for this expression is that it approximates the exact and Linnell's results for $M_\infty \sin \delta \geq 2$ quite well with $b = 1$. If b is allowed to vary so that a better fit to exact results is obtained, then $b = 3/4$ (Reference 31), and

$$\frac{C_p'}{(\gamma + 1) \sin^2 \delta} = 1.015 \qquad (II-12)$$

These "constants" are entirely empirical.

For a wedge, the inviscid pressure coefficient is given as

$$C_p = 1.015 \, (\gamma + 1) \sin^2 \delta + \frac{3}{4} \frac{p_\infty}{q_\infty} \qquad (II-13)$$

2. COMPRESSIBILITY EFFECTS

Using a reference temperature concept, the Blasius result for an incompressible boundary layer may be applied to the compressible boundary layer problem, thereby making it possible to calculate the local slope of the boundary layer. If and only if similarity exists can it be shown that

$$\frac{d\delta^*}{dx} = \frac{\delta^*}{\theta} \frac{d\theta}{dx} = \frac{\delta^*}{\theta} \frac{C_{f_e}}{2} \qquad (II-14)$$

where θ is the momentum thickness and C_{f_e} is the local coefficient of friction

$$C_{f_e} = \frac{\tau_w}{q_e} \qquad (II-15)$$

Employing the classical Blasius formulation for C_{f_e} and incorporating the reference property concept, Harney (Reference 20) gets, for the zero pressure gradient case,

$$\frac{C_{f_e}}{2} = 0.332 \frac{T_e}{T^*} \left(R\overset{*}{e}_{e_x} \right)^{-\frac{1}{2}} \qquad (II\text{-}16)$$

where

$$R\overset{*}{e}_{e_x} = \rho_e^* u_e x / \mu_e^* \qquad (II\text{-}17)$$

The displacement thickness, momentum thickness ratio can be expressed as

$$\frac{\delta^*}{\theta} = \frac{\int_0^1 \left(1 - \frac{\rho u}{\rho_e u_e} \right) d\left(\frac{y}{\delta_1} \right)}{\int_0^1 \frac{\rho u}{\rho_e u_e} \left(1 - \frac{u}{u_e} \right) d\left(\frac{y}{\delta_1} \right)} \qquad (II\text{-}18)$$

or by using a reference property concept in conjunction with a linear velocity profile

$$\frac{\delta^*}{\theta} = 2 \frac{T^*}{T_e} \left[1 - \frac{T_e}{2T^*} \right] \left(\frac{\delta^*}{\theta} \right)_{inc} \qquad (II\text{-}19)$$

where

$$\left(\frac{\delta^*}{\theta} \right)_{inc} = 3.00 . \qquad (II\text{-}20)$$

This may be compared with the Blasius result for $(\delta^*/\theta)_{inc}$, which is 2.591. Harney (Reference 20, Equation A-8) chose to use a value of 2.61 rather than either the linear or the Blasius values. It is shown in part 4 that by using the 2.61 factor in the calculation of the approximate temperature function, G, a good correlation results with the exact linear velocity profile analysis which uses the 3.00 value.

Combining Equations II-14, II-16, II-19, and II-20, it can be shown that

$$\frac{d\delta^*}{dx} = 1.992 \left[1 - \left(\frac{T_e}{2T^*}\right) \right] \left(Re^*_{e_x}\right)^{-\frac{1}{2}} \tag{II-21}$$

3. PRESSURE INTERACTION EFFECT

Harney (Reference 20) accounts for the nonzero pressure gradient effect, arising from the interaction of the viscous and inviscid flow fields, by a stretching transformation of the streamwise coordinate.

$$x^* = \rho \int_0^x \frac{1}{\rho} dx \tag{II-22}$$

This transformation produces local, flat plate similarity in the presence of small disturbance pressure gradients. It is this stretched coordinate which is used in place of the geometric coordinate in the reference Reynolds number

$$Re^*_{e_x} = Re^*_{e_{x^*}} = \frac{\rho^*_e u_e x^*}{\mu^*_e} \tag{II-23}$$

By using the zeroth order weak and strong interaction solutions as limits on the pressure variations, Harney found that $X^* = 2X/3$ in the strong limit and $X^* = X$ in the weak limit. For departures from the strong interaction limit, he used a linearized departure approximation (Reference 20, Equation 37)

$$\frac{x^*}{x} = \frac{2}{3} \left[1 + \frac{1}{4} \left(\frac{p_e}{p - p_e}\right) \right] \tag{II-24}$$

4. INVISCID, COMPRESSIBLE AND INTERACTION EFFECTS

Combining the results from parts 1, 2, and 3, it can be shown that

$$\left(Re_{e_x*}^*\right)^{-\frac{1}{2}} = \sqrt{\frac{2RT^*\mu^*}{u_e^3}} \left(\frac{p}{q_e}\right)^{-\frac{1}{2}} \left(\rho_e x^*\right)^{-\frac{1}{2}} \qquad (II\text{-}25)$$

and, after some manipulation, that

$$\frac{2RT^*\mu^*}{u_e^3} = \frac{2.339\times10^{-10}}{\left(1+\frac{198.6}{T^*}\right)} \left\{ \frac{\left(1+\frac{T_w}{T_0}\right)}{M_e^2} + \left(\frac{\gamma-1}{2}\right)(0.44\,r^*)\left[1+\frac{2.273}{r^*}\left(\frac{T_w}{T_0}\right)\right] \right\}^{\frac{1}{2}} \qquad (II\text{-}26)$$

Here the Eckert reference temperature (Reference 9) and Sutherland viscosity-temperature relations have been used. If this expression is combined with Equations II-21 and II-25, then

$$\frac{d\delta^*}{dx} = G'\left(\frac{p}{q_e}\right)^{-\frac{1}{2}}(\rho_e x^*)^{-\frac{1}{2}} \qquad (II\text{-}27)$$

where

$$G' = \frac{3.046\times10^{-8}}{\sqrt{1+\frac{198.6}{T^*}}}\left[1-\left(\frac{T_e}{2T^*}\right)\right] \left\{ \frac{\left(1+\frac{T_w}{T_0}\right)}{M_e^2} + 0.44\sqrt{P_r^*}\left(\frac{\gamma-1}{2}\right)\left[1+\frac{2.273}{\sqrt{P_r^*}}\left(\frac{T_w}{T_0}\right)\right] \right\}^{\frac{1}{2}} \qquad (II\text{-}28)$$

Here, the usual recovery factor approximation

$$r^* = \sqrt{P_r^*} \qquad (II\text{-}29)$$

has been made.

71

Harney, by making a number of simplifying assumptions, arrived at the expression*

$$G' = 3.84 \times 10^{-6} \left[1 + 2.6 \left(\frac{T_w}{T_0} \right) \right]^{\frac{3}{4}} \qquad (II-30)$$

The more exact result for G'(Equation II-28) indicates that it is dependent upon far more than just the T_w/T_0 ratio. To investigate this point further, a plot of the exact versus the approximate G' factor is shown in Figure 32. Considering Kendall's test (Reference 25), the approximate solution differs from the exact solution by only -0.94%, while the maximum G'deviation for Bertram's test (Reference 25) is 3.25%. The approximate value for G'based on the AFFDL data differs by a maximum of 4.14% from the exact solution, although for the data shown in Figure 7 the deviation is less than 1%. .A typical case with $T_0 = 2000°F$ and $M_\infty = 10$ is also shown in Figure 32. The maximum deviation from the exact solution is 7% at $T_w/T_0 = 0.8$.

The approximate G' relation (Equation II-30) agrees remarkably well with the more exact solution (Equation II-28) when the Mach number is low and the T_w/T_0 ratio approaches the adiabatic wall limit, and when the Mach number is high and the T_w/T_0 ratio is small. When the Mach number is high and the T_w/T_0 ratio approaches the adiabatic wall limit the correlation between the approximate and the exact values deteriorates somewhat but in general remains quite accurate. Regardless, the maximum deviation of the approximate Cp from the exact Cp is less than 0.7% for all the AFFDL data. Consequently, in this report the approximate theory, being much simpler, is used for data correlation.

---

*Harney's analysis also included the effects of a nonequilibrium freestream. Since these effects are not encountered in the experiments reported herein, they are not included in this report.
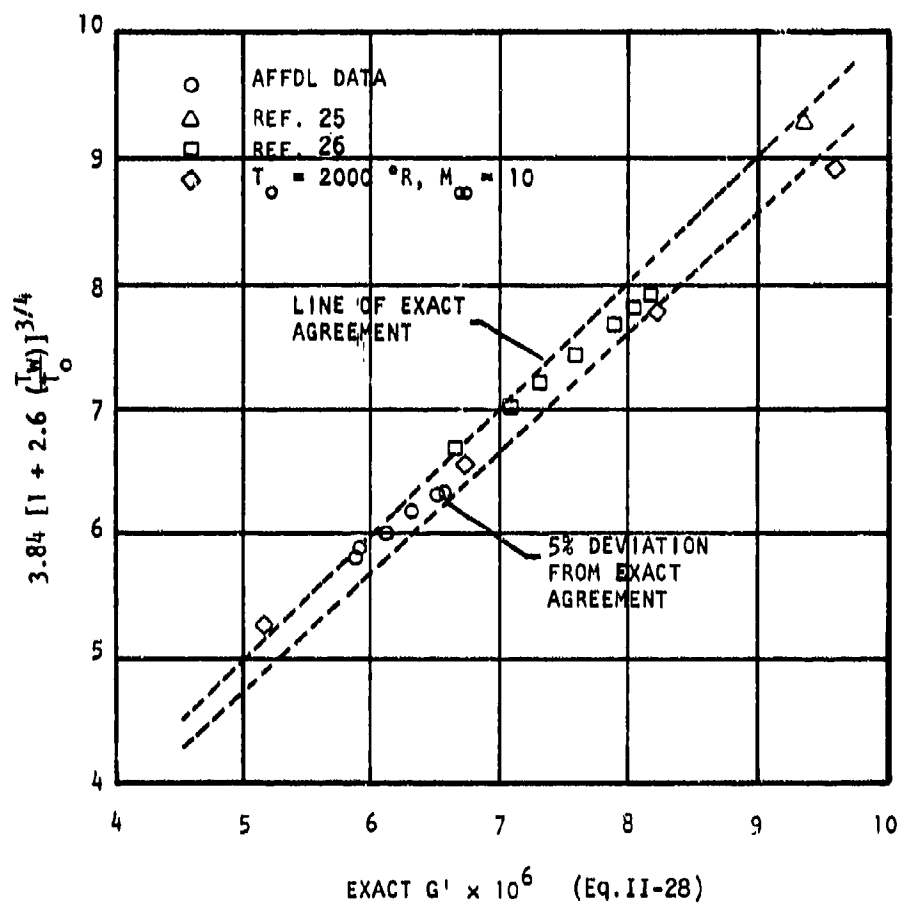
Figure 32.   Comparison of Exact vs Approximate Wall
Temperature Factor, G'

Equation II-27 may now be combined with Equation II-13 to get

$$c_p = 1.015(1+\gamma)\left(\delta_{inv} + \frac{d\delta^*}{dx}\right)^2 + \frac{3}{4}\frac{p_e}{q_e} \qquad (II-31)$$

or

$$\left[\frac{c_p - \frac{3}{4}\frac{p_e}{q_e}}{1.015(1+\gamma)}\right]^{\frac{1}{2}} = \delta_{inv} + G'\left(\frac{p}{q_e}\right)^{-\frac{1}{2}}(\rho_e x^*)^{-\frac{1}{2}} . \qquad (II-32)$$

Rearranging,

$$\left(c_p + \frac{p_e}{q_e}\right)^{\frac{1}{2}}\left(c_p - \frac{3}{4}\frac{p_e}{q_e}\right)^{\frac{1}{2}} = \left[1.015(1+\gamma)\right]^{\frac{1}{2}}\left[\left(c_p + \frac{p_e}{q_e}\right)^{\frac{1}{2}}\delta_{inv} + \frac{u_e}{u_e}G'(\rho_e x^*)^{-\frac{1}{2}}\right] .$$

$$(II-33)$$

For small angles of attack, the small disturbance assumption can be invoked

$$\frac{u_e}{u_e} \simeq 1 \qquad (II-34)$$

while for moderate angles of attack the right hand side of Equation II-33 is dominated by the

$$\left(c_p + \frac{p_e}{q_e}\right)^{\frac{1}{2}}\delta_{inv} \qquad (II-35)$$

term, and the effect of the small error introduced by assuming $u_e/u_\infty = 1$ is significant. With this approximation, Equation II-33 can be written as

$$\left(c_p + \frac{p_e}{q_e}\right)^{\frac{1}{2}}\left(c_p - \frac{3}{4}\frac{p_e}{q_e}\right)^{\frac{1}{2}} = \left[1.015(1+\gamma)\right]^{\frac{1}{2}}\left[\left(c_p + \frac{p_e}{q_e}\right)^{\frac{1}{2}}\delta_{inv} + G'(\rho_e x^*)^{-\frac{1}{2}}\right] .$$

$$(II-36)$$

5. FLAT PLATE ORIENTED PARALLEL TO THE FREESTREAM ($\delta_{inv} = 0°$)

For the zero angle of attack case, Equation II-36 simplifies even further

$$\left(c_p + \frac{p_\infty}{q_\infty}\right)^{\frac{1}{2}}\left(c_p - \frac{3}{4}\frac{p_\infty}{q_\infty}\right)^{\frac{1}{2}} = \left[1.015(1+\gamma)\right]^{\frac{1}{2}} G'(\rho_\infty x^*)^{-\frac{1}{2}} \qquad (II\text{-}37)$$

This equation reduces to a quadratic expression for the weak and strong interaction limits, and to a cubic expression for the linearized approximation for departures from the strong interaction limit. A more detailed analysis of the validity of the exact solution in comparison with an approximate solution is given in Appendix III, where it is shown that the simplified, approximate equation

$$c_p = \left[1.015(1+\gamma)\right]^{\frac{1}{2}} G'(\rho_\infty x^*)^{-\frac{1}{2}} \qquad (II\text{-}38)$$

gives a more reasonable result than the exact solution.

6. FLAT PLATE INCLINED TO THE FREESTREAM ($\delta_{inv} > 0°$)

For the nonzero angle of attack case, Equation II-36 has to be solved by iteration.

APPENDIX III

A COMPARISON OF EXACT AND APPROXIMATE SOLUTIONS FOR THE
BINARY SCALING PRESSURE COEFFICIENT ON SHARP FLAT PLATES
AT ZERO DEGREES ANGLE OF ATTACK

APPENDIX III

A COMPARISON OF EXACT AND APPROXIMATE SOLUTIONS FOR THE
BINARY SCALING PRESSURE COEFFICIENT ON SHARP FLAT PLATES
AT ZERO DEGREES ANGLE OF ATTACK

1. EXACT SOLUTIONS

The most general form of the expression for the pressure coefficient on sharp, flat plates at zero degrees angle of attack is (Appendix II, Equation II-36)

$$\left(c_p + \frac{p_\infty}{q_\infty}\right)^{\frac{1}{2}} \left(c_p - \frac{3}{4}\frac{p_\infty}{q_\infty}\right)^{\frac{1}{2}} = \left[1.015(1+\gamma)\right]^{\frac{1}{2}} \bar{G}(\rho_\infty x^*)^{-\frac{1}{2}} \qquad \text{(III-1)}$$

which may be squared to give

$$c_p^2 + \left(\frac{1}{4}\frac{p_\infty}{q_\infty}\right) c_p - \frac{3}{4}\left(\frac{p_\infty}{q_\infty}\right)^2 - \left[1.015(1+\gamma)\right]\bar{G}^2/(\rho_\infty x^*) = 0 \qquad \text{(III-2)}$$

This equation can be solved for Cp by employing the quadratic expression

$$c_p = \sqrt{\left(\frac{7}{8}\frac{p_\infty}{q_\infty}\right)^2 + \bar{G}^2\left[1.015(1+\gamma)\right]/(\rho_\infty x^*)} - \left(\frac{1}{8}\frac{p_\infty}{q_\infty}\right) \,. \qquad \text{(III-3)}$$

For the weak interaction limit $X^* = X$, and the strong interaction limit, $X^* = 2X/3$, the solutions are straightforward; however, for the linearized approximation about the strong interaction limit

$$x^* = \frac{2}{3} x \left[1 + \frac{1}{4}\left(\frac{p_\infty}{p - p_\infty}\right)\right] \,, \qquad \text{(III-4)}$$

A cubic solution is necessary. By substituting the linearized expression for X* into Equation III-3 and rearranging, we arrive at the cubic equation

$$c_p^3 + 2\left(\frac{1}{4}\frac{p_\infty}{q_\infty}\right)c_p^2 - \left\{11\left(\frac{1}{4}\frac{p_\infty}{q_\infty}\right)^2 + \left(\frac{3}{2}\right)\frac{\left[1.015(1+\gamma)\right]\dot{G}'^2}{(\rho_\infty x)}\right\}c_p - 12\left(\frac{1}{4}\frac{p_\infty}{q_\infty}\right)^3 = 0 .$$

$$\text{(III-5)}$$

It can be shown that this equation has three real and unequal roots.

The correct root is

$$c_p = 2\sqrt{-\frac{a}{3}}\cos\left(\frac{\phi}{3}\right) - \frac{1}{3}c \qquad \text{(III-6)}$$

where

$$a = -\frac{37}{3}\left(\frac{1}{4}\frac{p_\infty}{q_\infty}\right)^2 - \left(\frac{3}{2}\right)\frac{\left[1.015(1+\gamma)\right]\dot{G}'^2}{(\rho_\infty x)} \qquad \text{(III-7)}$$

$$b = \left\{\frac{\left[1.015(1+\gamma)\right]\dot{G}'^2}{(\rho_\infty x)} - \left(\frac{110}{27}\right)\left(\frac{1}{4}\frac{p_\infty}{q_\infty}\right)^2\right\}\left(\frac{1}{4}\frac{p_\infty}{q_\infty}\right) \qquad \text{(III-8)}$$

$$c = \frac{1}{2}\frac{p_\infty}{q_\infty} \qquad \text{(III-9)}$$

and

$$\cos\phi = -\frac{b}{2}\bigg/\sqrt{\left(\frac{-a^3}{27}\right)} \qquad \text{(III-10)}$$

2. APPROXIMATE SOLUTIONS

Employing the basic hypersonic assumption, $M_\infty \gg 1$, the left hand side of Equation III-1 becomes

$$\left(c_p + \frac{p_\infty}{q_\infty}\right)^{\frac{1}{2}} \left(c_p - \frac{3}{4}\frac{p_\infty}{q_\infty}\right)^{\frac{1}{2}} \simeq c_p \tag{III-11}$$

The validity of this approximation can be ascertained from Figure 33. With this approximation Equation III-1 simplifies considerably

$$c_p = \left[1.015(1+\gamma)\right]^{\frac{1}{2}} G'(\rho_\infty x^*)^{-\frac{1}{2}} \tag{III-12}$$

For the weak and strong interaction limits the solutions again are straightforward:

a. Weak interaction limit, $X^* = X$

$$c_p = \left[1.015(1+\gamma)\right]^{\frac{1}{2}} G'(\rho_\infty x)^{-\frac{1}{2}} \tag{III-13}$$

b. Strong interaction limit, $X^* = 2X/3$

$$c_p = \sqrt{\left(\frac{3}{2}\right)} \left[1.015(1+\gamma)\right]^{\frac{1}{2}} G'(\rho_\infty x)^{-\frac{1}{2}} \tag{III-14}$$

For the linearized departure from the strong interaction limit, a simple quadratic equation results:

$$c_p = \sqrt{\left(\frac{1}{8}\frac{p_\infty}{q_\infty}\right)^2 + \frac{3}{2}\left[1.015(1+\gamma)\right]G'^2/(\rho_\infty x)} - \left(\frac{1}{8}\frac{p_\infty}{q_\infty}\right) \tag{III-15}$$

c_p
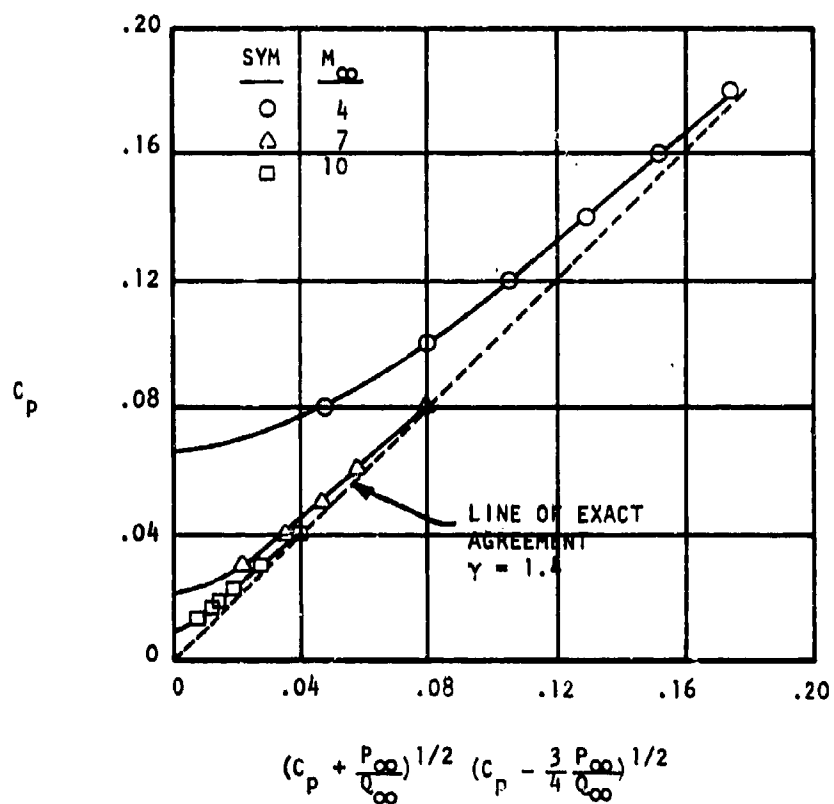
$$\left(C_p + \frac{P_\infty}{Q_\infty}\right)^{1/2} \left(C_p - \frac{3}{4} \frac{P_\infty}{Q_\infty}\right)^{1/2}$$

Figure 33. Comparison of C_p vs. $\left(C_p + \frac{p_\infty}{q_\infty}\right)^{1/2} \left(C_p - \frac{3}{4} \frac{p_\infty}{q_\infty}\right)^{1/2}$ for Various Freestream Mach Numbers

3. EVALUATION OF THE EXACT SOLUTION

A comparison of the exact and approximate solutions are shown in Figure 34 for three nearly identical wind tunnel conditions. On this figure is superimposed a line representing data sets from three separate wind tunnel tests. The data and the approximate solutions tend to Cp = 0 as the scaling factor, $(\rho_\infty x)^{-1/2}$, becomes very small. The approximate solution provides a better correlation with the data and with what one would expect a priori simply because the assumptions involved in the derivation of the approximate equation are consistent with the assumptions involved in obtaining the solution to this equation. As the Mach number becomes larger and larger the exact solution will approach the basic hypersonic, straight line result. (See also Figure 33). Only the approximate straight line solution will be considered in this report.
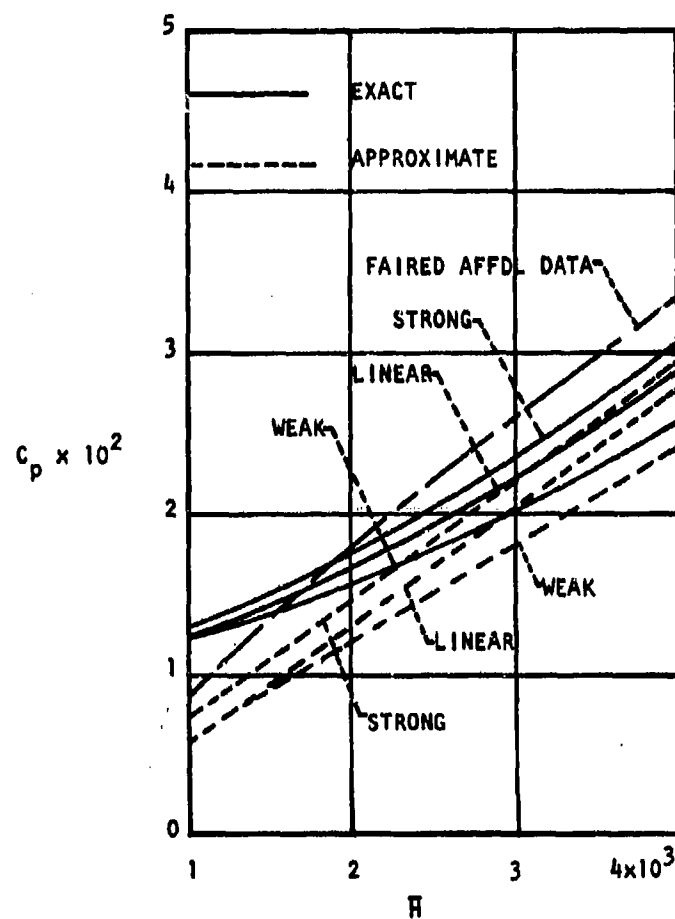
Figure 34. Comparison of Approximate vs Exact Binary Collision Solution at $\delta_{inv} = 0°$

REFERENCES

1. Marshall,E.M., and Funderburg, J. A., <u>Viscous Interaction Effects-Pressure Data on Flat Plate at Mach = 10.0</u>, AFFDL TM 71-21 FXG, Air Force Flight Dynamics Laboratory, Wright-Patterson Air Force Base, Ohio, August 1971.

2. Czysz, P., <u>The High Temperature Hypersonic Gasdynamics Facility Estimated Mach Number 6 Through 14 Performance</u>, ASD-TDR-63-456, Air Force Flight Dynamics Laboratory, Wright-Patterson Air Force Base, Ohio, June 1963.

3. Schnabel, C., Smith, R. R., and Dahlem, V., III, <u>Performance Estimates For The AFFDL Pebble Bed Heated Hypersonic Wind Tunnel</u>, FDM TM 67-3, Air Force Flight Dynamics Laboratory, Wright-Patterson Air Force Base, Ohio, July 1967.

4. Ames Research Staff, <u>Equations, Tables, and Charts for Compressible Flow</u>, NACA Report 1135, 1953.

5. Chapman, D. R., and Rubesin, M. W., "Temperature and Velocity Profiles in the Compressible Laminar Boundary Layer with Arbitrary Distribution of Surface Temperature", <u>Journal of the Aeronautical Sciences, Vol. 16, No. 9</u>, pp. 547-565, September 1949.

6. Monaghan, R. J., " On the Behavior of Boundary Layers at Supersonic Speeds", <u>Fifth International Aeronautical Conference, Los Angeles-1955</u>, (IAS-RAeS Proceedings) p. 277-315.

7. Crocco, L., "Boundary Layer of Gases Along a Flat Plate", <u>Seminario Matenatico Rendiconti</u>, University of Rome, Italy, Vol. 2, p. 138,

8. Cheng, H. K., Hall, J. G. Golian, T. C., and Hertzberg, A., "Boundary Layer Displacement and Leading-Edge Bluntness Effects in High-Temperature Hypersonic Flow", <u>Journal of the Aerospace Sciences, Vol. 28, No. 5</u>, May 1961.

9. Eckert, E. R. G., <u>Survey on Heat Transfer at High Speeds</u>, ARL 189, December 1961, AD 274109.

10. Lees, L., <u>Hypersonic Flow, Fifth International Aeronautical Conference</u> (Los Angeles, Calif., June 20-23, 1955), Inst. Aero. Sci., Inc., 1955, pp. 241-276.

11. Lees, L. "Influence of the Leading-Edge Shock Wave on the Laminar Boundary at Hypersonic Speeds", <u>Jour. Aero. Sci., Vol. 23</u>, No.6 June 1956, pp 594-600, 612.

REFERENCES (CONT)

12. Lees, L., and Probstein, R. F., Hypersonic Viscous Flow Over A Flat Plate, Princeton University Aeronautical Engineering Lab, Report No. 195, 20 April 1952.

13. Lees, L., and Probstein, R. F., Hypersonic Flows of a Viscous Fluid, 1953, AD 218 755.

14. Bertram, M. H., An Approximate Method For Determining the Displacement Effects and Viscous Drag of Laminar Boundary Layers in Two-Dimensional Hypersonic Flow, NACA TN 2773, 1952.

15. Li, T. Y., and Nagamatsu, H. T., "Shock Wave Effects on the Laminar Skin Friction of an Insulated Flat Plate at Hypersonic Speeds," Jour Aero. Sci., Vol. 20, No. 5, May 1953, pp. 345-355.

16. Hays, W. D., and Probstein, R. F., Hypersonic Flow Theory, Academic Press, New York and London, 1959.

17. Moore, F. K., "On Local Flat-Plate Similarity in the Hypersonic Boundary Layer", J. Aero. Sci., Vol. 28, No. 10, pp. 753-762, October 1961.

18. Dewey, C. F., Jr., "Use of Local Similarity Concepts in Hypersonic Viscous Interaction Problems", AIAA Journal, Vol. 1, No. 1, January 1963.

19. Birkhoff, G., Hydrodynamics, A Study in Logic, Fact and Similitude, Princeton University Press, 1960.

20. Harney, D. J., "Slender Body Aerodynamic Testing Potential of High Energy Wind Tunnels", AIAA Paper No. 68-383, AIAA 3rd Aerodynamic Testing Conference, April 8-10, 1968.

21. Harney, D. J., and Petrie, S. L., A Flat Plate Study of the Binary Scaling of Viscous Hypersonic Flow, AFFDL-TR-71-104, Air Force Flight Dynamics Laboratory, Wright-Patterson Air Force Base, Ohio, August 1971.

22. Harney, D. J., Petrie, S. L., Hypersonic Surface Pressure and Heat Transfer on Slender Bodies in Variable Composition and Nonequilibrium Atmospheres, AFFDL-TR-70-31, Air Force Flight Dynamics Laboratory, Wright-Patterson Air Force Base, Ohio, April 1970.

23. Li, T. Y. and Nagamatsu, H. T., "Hypersonic Viscous Flow on Non-Insulated Flat Plate", Proc. 4th Midwestern Conference on Fluid Mechanics, Purdue University, pp. 273-287, Sept. 8-9, 1955.

REFERENCES (CONT)

24. Moulic, E. S., and Maslach, G. J., "Induced Pressure Measurements On A Sharp-Edged Insulated Flat Plate in Low Density Hypersonic Flow", Rarefied Gasdynamics, Supplement 4, Vol. II, pp. 971-992, Academic Press, New York, London, 1967.

25. Kendall, J. M. Jr., "An Experimental Investigation of Leading-Edge Shock-Wave-Boundary-Layer Interaction at Mach 5.8, Journal of the Aeronautical Sciences, Vol. 24, No. 1, pp 47-56, January 1957.

26. Bertram, M. H. , Boundary Layer Displacement Effects in Air at Mach Numbers of 6.8 and 9.6, NASA TR R-22, 1959.

27. McCroskey, W. J., Bogdonoff, S. M., and McDougall, J. G., "An Experimental Model For the Leading Edge of a Sharp Flat Plate In Rarefied Hypersonic Flow", AIAA Paper No. 66-31, AIAA 3rd Aerospace Sciences Meeting, New York, New York, Jan 24-26, 1966.

28. Pan, Y. S., and Probstein, R. F., "Rarefied-Flow Transition at a Leading Edge", Proceedings of International Symposium on Fundamental Phenomena in Hypersonic Flow, Cornell University Press, 1966.

29. Vas, I. E., Iacavazzi, C., Carlomagno, G., and Bogdonoff, S. M., "Effect of Body Inclination On the Merging of a Hypersonic Low Density Flow Over Sharp Two-Dimensional Linear Bodies", Rarefied Gasdynamics, Supplement 5, Vol. 1, pp. 501-508, Academic Press, New York, London 1969.

30. McCrosky, W. J., Bogdonoff, S. M., and Genchi, A. P., "Leading Edge Flow Studies of Sharp Bodies in Rarefied Hypersonic Flow", Rarefied Gasdynamics, Supplement 4, Vol. II, pp 1047-1066, Academic Press, New York, London, 1967.

31. Harney, D. J., A Simple Aerodynamic Rule For Hypersonic Small Disturbance Flows, AFFDL-TR-68-4, Air Force Flight Dynamics Laboratory, Wright-Patterson Air Force Base, Ohio, March 1968.

32. Hilsenrath, J., et al, Tables of Thermal Properties of Air, National Bureau of Standards Circular 564, United States Department of Commerce, November 1955.

33. Hirschfelder, J. O, Curtis, C. F., and Bird, R. B., Molecular Theory of Gases and Liquids, John Wiley and Sons, New York, 1954.

34. Linnell, R. D., "Two-Dimensional Airfoils in Hypersonic Flows", Jour. Aero. Sci., Vol. 16, pp. 22-30, 1949.